AD_____

Award Number: W81XWH-12-1-0279

TITLE: Synthetic Lectins: New Tools for Detection and Management of Prostate Cancer

PRINCIPAL INVESTIGATOR: Paul R. Thompson

CONTRACTING ORGANIZATION: The Scripps Research Institute
                                La Jolla, CA 92037-1000

REPORT DATE: August 2014

TYPE OF REPORT: Annual

PREPARED FOR: U.S. Army Medical Research and Materiel Command
                Fort Detrick, Maryland 21702-5012

REPORT DOCUMENTATION PAGE

Form Approved
OMB No. 0704-0188

Public reporting burden for this collection of information is estimated to average 1 hour per response, including the time for reviewing instructions, searching existing data sources, gathering and maintaining the data needed, and completing and reviewing this collection of information. Send comments regarding this burden estimate or any other aspect of this collection of information, including suggestions for reducing this burden to Department of Defense, Washington Headquarters Services, Directorate for Information Operations and Reports (0704-0188), 1215 Jefferson Davis Highway, Suite 1204, Arlington, VA 22202-4302. Respondents should be aware that notwithstanding any other provision of law, no person shall be subject to any penalty for failing to comply with a collection of information if it does not display a currently valid OMB control number. **PLEASE DO NOT RETURN YOUR FORM TO THE ABOVE ADDRESS.**

1. REPORT DATE	2. REPORT TYPE	3. DATES COVERED
August 2014	Annual	19 Jul 2013 - 18 Jul 2014

4. TITLE AND SUBTITLE	5a. CONTRACT NUMBER
Synthetic Lectins: New Tools for Detection and Management of Prostate Cancer	
	5b. GRANT NUMBER W81XWH-12-1-0279
	5c. PROGRAM ELEMENT NUMBER

6. AUTHOR(S)	5d. PROJECT NUMBER
Paul R. Thompson, John J. Lavigne	
	5e. TASK NUMBER
	5f. WORK UNIT NUMBER
E-Mail: Paul.Thompson@umassmed.edu, Lavigne@sc.edu	

7. PERFORMING ORGANIZATION NAME(S) AND ADDRESS(ES)	8. PERFORMING ORGANIZATION REPORT NUMBER
The Scripps Research Institute La Jolla, CA 92037-1000	

9. SPONSORING / MONITORING AGENCY NAME(S) AND ADDRESS(ES)	10. SPONSOR/MONITOR'S ACRONYM(S)
U.S. Army Medical Research and Materiel Command Fort Detrick, Maryland 21702-5012	
	11. SPONSOR/MONITOR'S REPORT NUMBER(S)

12. DISTRIBUTION / AVAILABILITY STATEMENT
Approved for Public Release; Distribution Unlimited

13. SUPPLEMENTARY NOTES

14. ABSTRACT
Among US men, prostate cancer is the most common cancer (besides non-malignant skin cancer), afflicting over 200,000 each year, and is the second leading cause of cancer-related death, over 30,000 per year. Thus, our long term goal is to develop synthetic lectin (SL) arrays for the detection and diagnosis of prostate cancer. We are pursuing this goal because healthy and diseased cells produce different biomarkers, which provide unique signatures by which these cells can be distinguished. Taking advantage of the fact that aberrant protein glycosylation is a hallmark of cancer; we propose to develop a novel sensor platform that can be used to detect Cancer Associated Glycans/Glycoproteins for the diagnosis of prostate cancer. The basis of this diagnostic is the differential display of boronic acids on peptides and peptoids. Boronic acids are used because they form covalent yet reversible bonds with specific structural motifs (i.e., diols) present on all Cancer Associated Glycans/Glycoproteins. The covalent interaction increases the affinity of the SL for the target Cancer Associated Glycans/Glycoproteins, while the peptide/peptoid backbone and preorganization of the boronic acids define the selectivity of binding. Building on preliminary data, which demonstrated the ability to identify synthetic lectins, assemble them into an array, and discriminate between normal, cancerous and metastatic colon cancer cell lines, we will: **(1)** generate synthetic lectins that recognize specific Cancer Associated Glycans/Glycoproteins; **(2)** probe the biochemical and biophysical basis for the glycan-SL interactions to enhance binding affinities and selectivities; and **(3)** create multi-component sensor arrays to differentiate cell and tissue types to diagnose and monitor prostate cancer. The development of these synthetic lectins is highly significant because they can be used to generate an array based diagnostic that has the potential to revolutionize the early diagnosis of prostate cancer.

15. SUBJECT TERMS
Lectins, prostate cancer, glycans, glycosylation.

16. SECURITY CLASSIFICATION OF:			17. LIMITATION OF ABSTRACT	18. NUMBER OF PAGES	19a. NAME OF RESPONSIBLE PERSON USAMRMC
a. REPORT U	**b. ABSTRACT** U	**c. THIS PAGE** U	UU	42	**19b. TELEPHONE NUMBER** *(include area code)*

Table of Contents

Introduction

The overall goal of this proposal is to develop synthetic lectins (SLs) that bind to prostate cancer associated glycans and glycoproteins (CAGs). These studies are being pursued to develop this methodology into a robust system that can diagnose and monitor the stage of prostate cancer. Related to the proposed system, aberrant glycosylation is a hallmark of cancer and, as such, the differential display of boronic acid moieties on peptides and peptoids will allow for monitoring the changes (over- or neoexpression of CAGs) associated with oncogenesis and metastasis, thereby providing a new paradigm for the development of a prostate cancer diagnostic. AIM 1 describes a library based approach for the discovery of SLs targeting CAGs. AIM 2 describes biochemical and biophysical approaches to identify the factors that are required for the selective recognition of CAGs. It is expected that the results of these studies will provide information that will allow us to improve the design of the libraries described in AIM 1, towards second and third generation libraries. In AIM 3, selective and cross-reactive SLs will be assembled into an SL-based array. The efficacy of this array will be evaluated using both prostate cancer derived CAGs and actual cell lines.

Keywords

synthetic lectin, lectin, prostate cancer, glycan, glycoprotein, glycosylation, cancer associated glycoprotein (CAG), tumor-associated carbohydrate antigen (TACA)
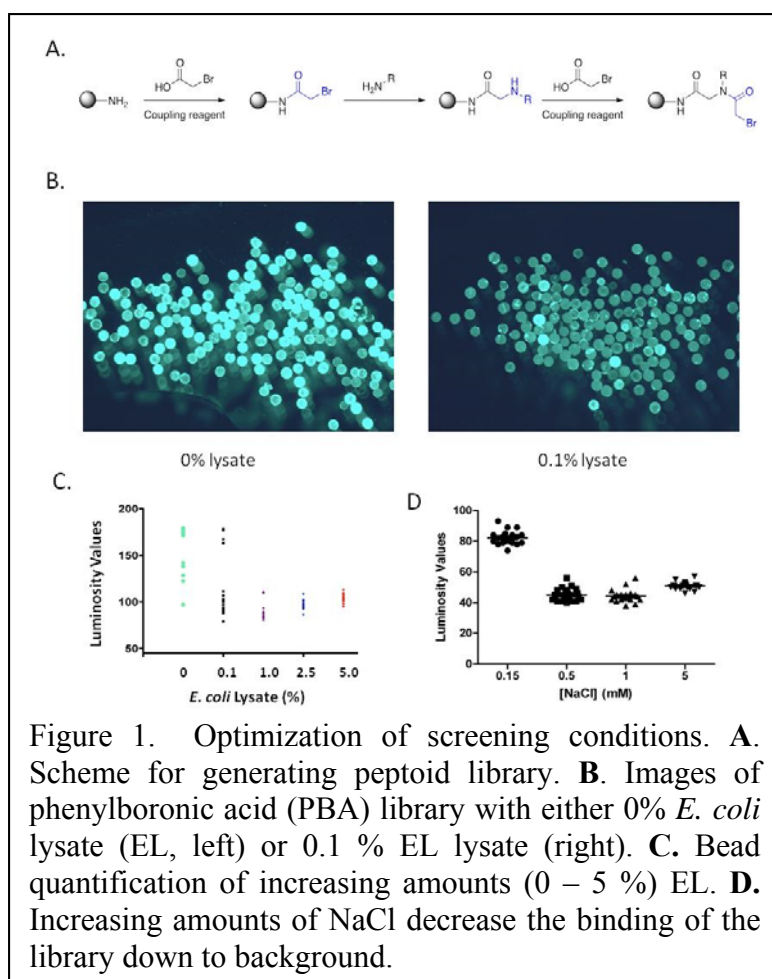
Overall Project Summary

Significant progress has been made in the prior funding period. While continuing to learn a great deal about how our SLs are binding with glycan and glycoproteins, we have also made great headway towards assessing the utility of a SL-Array to respond to secreted glycoproteins and human tissue samples. In consultation with clinical colleagues, we have made strides towards simplifying the analysis platform/method and in working with statistical collaborators we are continuing to improve the robustness of our analysis while reducing sources of interface variation. Specifically, we have been able to move our bead-based readout from a fluorescence microscope to using a standard flow-based system (e.g. fluorescence activated cell sorter – FACS) while maintaining a significant portion of the assay validity. Furthermore, we have been able to demonstrate that the patterns generated by our SL Array responding to cell membrane extracts from cultured cells mimic those patterns obtained when analyzing the culture media from those same cell lines, providing support for the concept of creating a serum-based diagnostic. Similarly, we have begun to study glycosylation patterns from human tissue samples using our SL Array and have obtained excellent discrimination between matched healthy and cancerous tissues. In addition, we are continuing to develop and improve the screening methods used to identify new SLs. To drive our efforts towards more biological and disease relevant models, we have used cell membrane extracts rather than purified proteins as the target component of our library screening method. We have also identified a novel dual-label competitive binding screening assay that also relies on using cell membrane extracts. Because of our association with and proximity to the Center for Colon Cancer Research (CCCR) at the University of South Carolina (USC), a great deal of our initial, method development efforts have used colon cancer associated cell lines and tissue samples. As we have previously demonstrated and is discuss below, once the "bugs" have been worked out using colon cancer associated samples, the transition to prostate cancer related samples has been straightforward.

Task 1. Use a library-based approach to identify synthetic lectins that bind to prostate cancer associated glycans/glycoproteins (CAGs). Note that this aim will continue over the life of the grant to continuously identify more selective and useful SLs. (Months 1-36)

Initiating PI:

Task 1 a): Synthesize bead based peptoid libraries that incorporate phenylboronic acid moieties. (Months 1-4)

Peptoid libraries were constructed using 9 amine building blocks (diversity = 9^5; 5.9 x 10^4 members) using the scheme depicted in Figure 1A. Briefly, bromoacetic acid was coupled using DIC to Tentagel –NH$_2$ beads already coated with our MRBB linker sequence. The beads were split and the 9 different amines were added to equal amounts of beads and reacted in DMF. The beads were then washed, re-pooled and treated with bromoacetic acid

Figure 1. Optimization of screening conditions. **A**. Scheme for generating peptoid library. **B**. Images of phenylboronic acid (PBA) library with either 0% *E. coli* lysate (EL, left) or 0.1 % EL lysate (right). **C.** Bead quantification of increasing amounts (0 – 5 %) EL. **D.** Increasing amounts of NaCl decrease the binding of the library down to background.

5

and DIC to couple the second diversity element. The Dde protecting group was selectively removed using hydrazine to uncover the primary amine to be conjugated to phenylboronic acid (PBA). PBA installation was verified using ARS and several beads were randomly selected for library quality evaluation.

With the synthesized libraries in hand, we turned our attention to identifying ideal screening conditions. Our goal was to identify stringent conditions so we could identify highly selective hits from our libraries. Based on previous studies,[1] we used *E. coli* lysates (EL) to both pre-block the beads and minimize non-specific interactions during analyte incubation. Figure 1B shows the drastic decrease in fluorescence when adding 0.1% EL to the screening buffer. Indeed, an EL gradient (Figure 1C) identified 0.1% EL as the optimal concentration since higher concentrations showed to strong of a decrease in fluorescence. We then optimized the salt concentrations (Figure 1D) and determined that 150 mM NaCl is ideal.

Task 1 b): Screen peptoid libraries with prostate cancer associated glycoproteins and complex glycans to identify highly selective and cross-reactive synthetic lectin (SL) hits. (Months 3-36)

To identify SLs that are specific for CAGs (Figure 4A), we designed a screening platform that used biotinylated complex carbohydrates conjugated to fluorescently labeled streptavidin (SA) (Figure 4B). Briefly, a series of biotinylated carbohydrates (i.e., sialyl Lewis X, sialyl Lewis A, Lewis X and Lewis A) were obtained from the Consortium of Functional Glycomics (CFG). Because of our previous success with peptide library screening, we initially optimized our screening conditions using phenylboronic acid based peptide libraries instead of peptoid based ones incorporating either the phenylboronic acid or benzoboroxole moieties. For this assay, we pre-incubated the CFG glycans with FITC-streptavidin for 1 h in a 4:1 glycan-SA ratio then added this complex to our PBA-peptide library in screening buffer. Using this method, we identified 2 hits when screening with sLe^x as the target glycan. These hits were sequenced and had the following sequences: sLe^{x}1 = MRBB–LD*RFRD*L-Ac and sLe^{x}2 = MRBB–RD*RWVD*Y-Ac. In addition to validating this screening modality for identifying both peptide and peptoid based libraries, further analyses demonstrate that these hits bind sialyl Lewis X better than Le^x or either of the Le^a derivatives (see below).

During the second year of funding we continued to focus on building SLs from peptides due to the immense success we have had with this structural motif. As such we screened our fixed-position-library (FPL) against fluorescein labeled prostate specific antigen (FITC-PSA). While the diagnostic utility of PSA has demonstrated little to no validity as a biomarker for prostate cancer, we chose PSA for screening because it displays many of the glycans overexpressed in prostate cancer and it is commercially available. Briefly, 2 mg of library beads were washed with PBSG twice and then incubated with 1% BSA in PBSG for 15 minutes to reduce nonspecific background binding. The solution was removed from the beads and 0.01 mg/ml of FITC-PSA in PBS was added. The beads were incubated with this solution for 20 hours at room temperature, after which the supernatant was removed and the resin washed with PBS three times before imaging using fluorescence microscopy. Figure 2 depicts

Figure 2. The green channel from a typical image from screening the FPL with FITC-PSA. The bright bead indicates a "hit" for binding PSA.

the green channel from a typical image from this screening protocol. Note that the brighter bead would be classified as a "hit." We are currently working to sequence these hits using MALDI-MS.
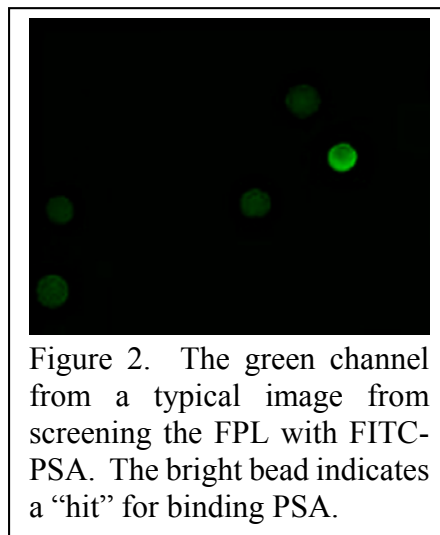
We have alternatively begun to screen our libraries with cell membrane extracts as well as using competitive binding assays between cell membrane extracts from normal and cancerous prostate cell lines. For all of the work discussed below, we have used RWPE-1 cells as our normal/healthy cell line and PC3 as our cancerous cell line. Figure 3A shows a normalized binning chart for screening our FPL with rhodamine labeled membrane extracts (red diamonds) or fluorescein labeled membrane extracts (green diamonds).

Differentiation between what would be classified as "hits" (indicated within the blue box) and "non-specific background binding SLs is sufficient to obtain acceptable hit rates under 10%.

In the competitive binding screen, one sample is labeled with fluorescein while the other is labeled with rhodamine. In our current analysis, our samples are the cell membrane extracts from PC3 and RWPE-1. Each cell membrane extract was separately labeled with each dye to produce R-RWPE-1, F-RWPE-1, R-PC3, and F-PC3; where R = rhodamine, F = fluorescein. A portion of the FPL was then incubated separately with each cell membrane extract listed above (i.e. alone) and with all possible combinations in a 1:1 w/w ratio.

Figure 3B shows individual color channels from images taken of a portion of the FPL binding to a mixture of F-RWPE-1 and R-PC3 imaged under the appropriate filters for each dye, i.e. DSR for rhodamine (red channel) and GFP3 for fluorescein (green channel). Each image is of the same beads, just taken using a different emission filter. Note that the bead indicated by the yellow arrow in the green image is brighter than the other beads relative to the brightness of this same bead in the red image. This indicates that the SL attached to this bead binds more tightly to the fluorescein labeled analyte than to the rhodamine labeled analyte. Figure 3C expresses this more quantitatively, showing the fold increase in brightness for the six brightest beads in each image with respect to the average background binding. Notice that most of the intensities are close to one, indicating that these beads are in general of equal brightness and close to the average bead intensity. However, the bead labeled "4" displays nearly a 2-fold enhancement in binding to F-RWPE-1 compared to the other beads binding to F-RWPE-1 as well as compared with all of the beads binding to R-PC3, and corresponds to the bead indicated by the yellow arrow.
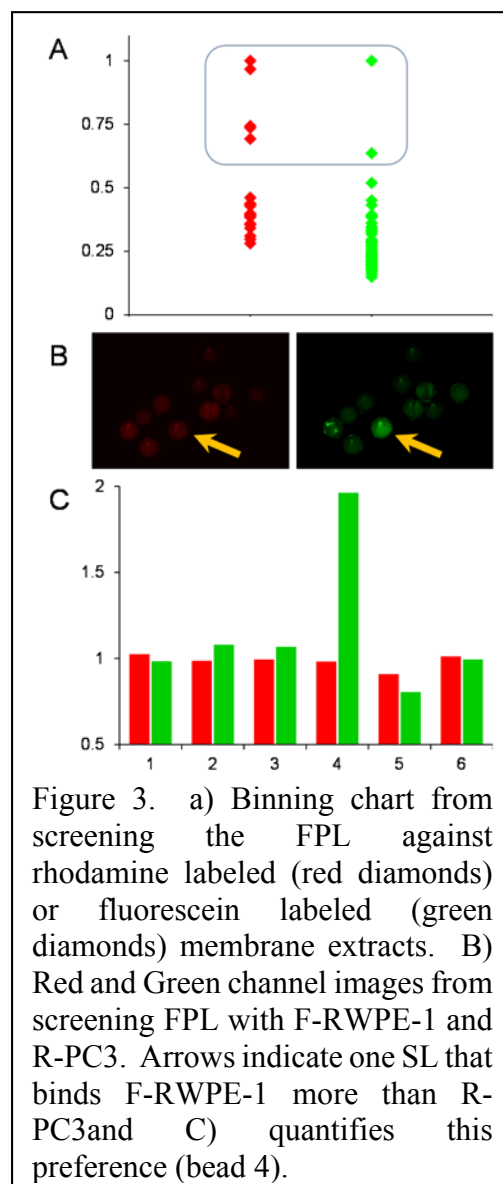

Figure 3. a) Binning chart from screening the FPL against rhodamine labeled (red diamonds) or fluorescein labeled (green diamonds) membrane extracts. B) Red and Green channel images from screening FPL with F-RWPE-1 and R-PC3. Arrows indicate one SL that binds F-RWPE-1 more than R-PC3 and C) quantifies this preference (bead 4).

Based upon screening our FPL with individual and mixed prostate derived cell membrane extracts, five new sequences have been identified, Table 1. Most significantly, these SLs were identified from screening our library with known prostate associated samples. Most excitingly, these SLs were identified from an incredibly heterogeneous mix of membrane supported proteins and glycoproteins, all labeled with a fluorescent dye. Furthermore, nearly half of these sequences came from mixtures of different incredibly heterogeneous cell membrane extracts, and still some degree of selectivity in binding was achieved! We are currently continuing to evaluate the selectivity of binding for these new SLS as well as assessing their utility as part of our SL Array.

Table 1. Sequences of SLs identified against prostate derived cell line membrane extracts.

SL Hit	Sequence	Cell Line Screened	Cell Line Selectivity
SL10	H$_2$N-RLD*ARSD*G-BBRM-resin	F-PC3	- -
SL11	H$_2$N-RLD*YLTD*R-BBRM-resin	F-RWPE-1/R-PC3	PC3
SL12	H$_2$N-RLD*GFYD*Q-BBRM-resin	F-RWPE-1/R-PC3	RWPE-1
SL13	H$_2$N-RTD*GLAD*V-BBRM-resin	F-RWPE-1	- -
SL14	H$_2$N-RYD*RASD*V-BBRM-resin	R-PC3	- -

7

Task 1 c): Upon identifying ≥5 hits, we will sequence, resynthesize, and determine their selectivity of identified hits towards the target that they were selected against as well as the other prostate cancer associated glycoproteins and complex glycans. (Months 3-36)

We set out to validate our two PBA-peptide hits by first resynthesizing the two hits identified in (Task 1b), sLe^{x}1 and sLe^{x}2. We then screened these hits against Le^x, Le^a and sLe^a (Figure 4A) and determined that both of the hits bind sLe^x better than Le^x or either of the Le^a derivatives (Figure 4C). These results are encouraging and will be expanded as the number of hits increases after additional rounds of screening.

In the second year of funding we have been able to sequence SLs from our fixed-position library using traditional Edman degradation techniques without removal of the boronic acid moiety. As previously discussed, we accepted the low success rate for sequencing hits using MALDI-MS-MS (~40%), and looked forward to using the
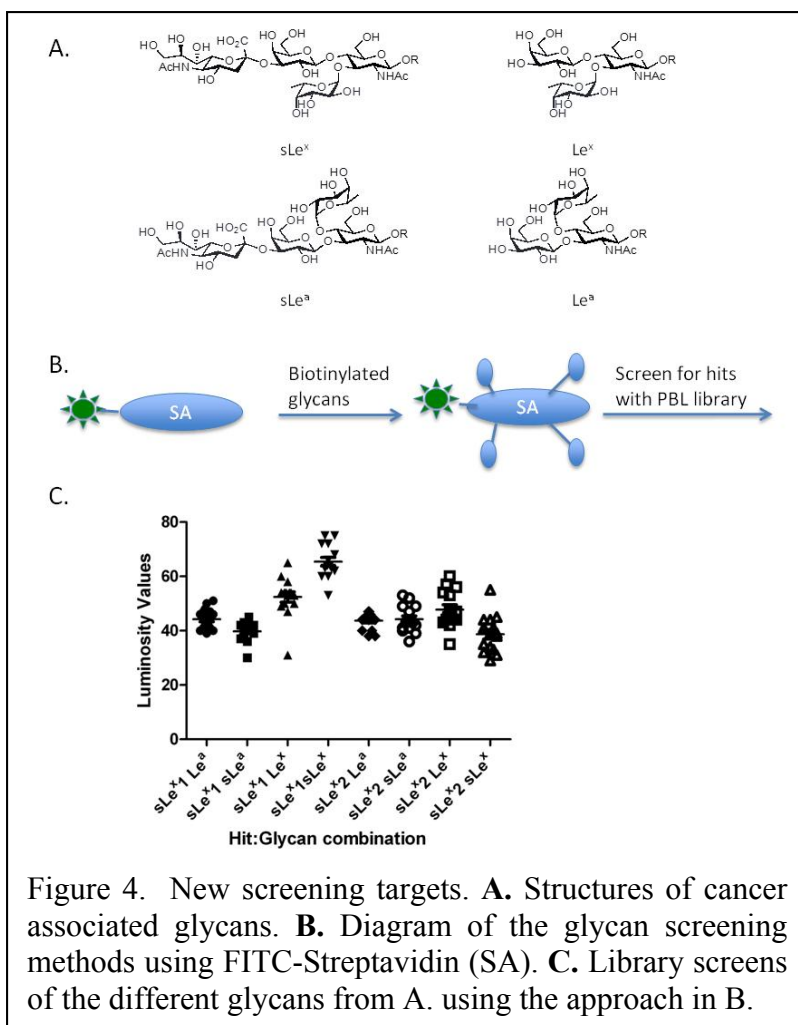

Figure 4. New screening targets. **A.** Structures of cancer associated glycans. **B.** Diagram of the glycan screening methods using FITC-Streptavidin (SA). **C.** Library screens of the different glycans from A. using the approach in B.

Orbi-Trap MS where we were able to obtain enhanced sensitivity and seemingly better sequencing efficiency. However, the observed increase in sensitivity often hindered our analysis by introducing higher background signal compared to MALDI-MS and thereby complicated the MS-MS analysis. Consequently, when provided the opportunity to evaluate using Edman degradation methods to sequence our SLs we enthusiastically tried it. The most significant change made to our design was that we could no longer acylate the N-terminus of our SLs, because to do so would end the possibility of using this technique. Thus a new library was synthesized using the split-and-pool protocol previously described. The primary modification from prior library syntheses was that instead of cleaving the Fmoc and acylating the terminal amine after coupling the final R; the Dab(ivDde) protecting groups were removed using hydrazine and the boronic acid groups were introduced via reductive amination prior to removing the Fmoc protecting group. The new general sequence for this fixed-position SL library is H$_2$N-R-X-D*-X-X-X-D*-X-B-B-R-M-resin, where X denotes a randomized amino acid chosen from R, A, G, V, N, Q, L, F, S, Y, T; while D* indicates diaminobutanoic acid with a 2-methyl phenyl boronic acid attached.

Perhaps the most compelling argument for switching from MS-based sequencing to Edman-based analysis is that there is no requirement to remove the boronic acids from the SL prior to sequencing. When using MALDI-MS we found that oxidation of the boronic acid, followed by cleavage of the resulting 2-methylphenol simplified our analyses. However, when using the Orbi-Trap MS we noticed not only removal of our phenyl boronic acid (PBA), but also partial and irregular cleavage of our SL backbone. This again only served to complicate our analysis when using data from the Orbi-Trap. In our first efforts using Edman degradation to sequence our SLs we obtained beautiful data for the SL peptide sequence that had never been

coupled with the boronic acids (as would be expected), including a new peak in the corresponding LC traces associated with Dab. However, the Edman-based sequencing results of known sequences after removal of the PBA showed the presence of numerous amino acids in each cycle, indicating that the SL peptide backbone had been partially hydrolyzed during the removal of the PBA. Control studies confirmed that incomplete coupling while synthesizing the SL was not to blame for this result. Consequently, we decided to evaluate this approach without removing the PBA groups. In the case of the fixed-position library, we know where the D* residues are and since we only need to know the identity of the five randomized amino acids before, between and after these building blocks the Edman-based approach should work
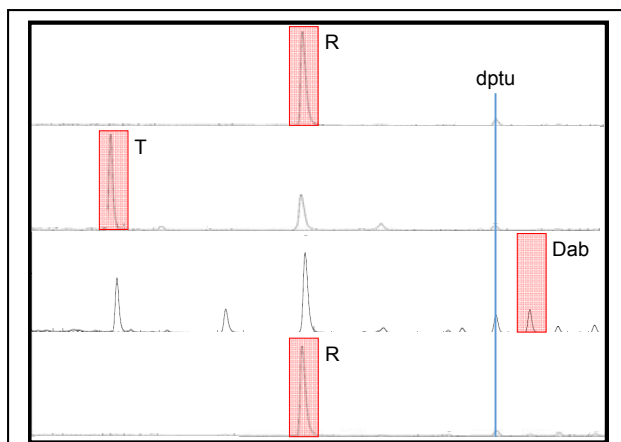

Figure 5. LC traces for the first 4 cycles of Edman degradation of SL2. The first 4 residues from the N-terminus are: R-T-Dab-R. Note the new peak for Dab in the third trace.

as long as the boronic acids do not interfere with the phenylisothiocyanate chemistry (Figure 5). Remarkably, the PBA does not appear to interfere with the analysis and in fact a new peak is observed in the LC trace that is consistent with the D* moiety (Figure 5), thereby opening the door for the use of completely randomized libraries with the ability to sequence the D* residues. Using this approach, we have identified four new SLs from library screens using prostate cancer associated glycoproteins and cell membrane extracts (Table 1).

Partnering PI:

Task 1 a): Synthesize bead-based peptide libraries that incorporate phenylboronic acid moieties. (Months 1-4)

Two peptide-based fixed-position libraries were synthesized on Tentagel resin analogous to those previously described.[2] The effectiveness of the coupling was assessed using MALDI-MS in the past, here however, we ran into difficulties. From all of our efforts, our MS analysis consistently indicated incomplete deprotection of the iv-Dde protecting groups on the Dab side-chains (where boronic acids are attached). This appeared to be a significant portion of the product, composing up to 60%. Moreover, our MS analysis frequently suggested that we were getting incomplete coupling of the first Dab moiety. These were problems we had not encountered previously, yet appeared to be an issue when even re-synthesizing known SLs.

Consequently, we thoroughly evaluated the quality of the batches of TentaGel resin, hydrazine (used to deprotect the iv-Dde) and Fmoc-Dab(iv-Dde)-OH from the vendors. Note that we were using the same vendors as we had in the past. No apparent anomalies were detected in these reagents. Furthermore, upon a detailed investigation of the literature, we identified much "controversy" and similar problems were indicated with respect to deprotecting the iv-Dde protecting group.

We thus opted to re-evaluate our synthetic approach and tried different side-chain amine protecting groups on Dab including alloc and MTT. From these studies, we determined that the deprotection of alloc was sensitive to water and oxygen, making it difficult to work with at times. Furthermore while the MTT group was easy to deprotect, amino acids with this group on the side-chain were often difficult to couple to the resin due to the size of the MTT group and increased steric interactions.

Interestingly, when we synthesized SL5 on a cleavable Rink Amide Resin using Fmoc-Dab(iv-Dde)-OH, we were able to confirm the presence of fully deprotected SL5 as the major product using MALDI-MS. Next, we more rigorously investigated the relative ratios of protected and deprotected SL5 from the TentaGel resin using LC-MS. Remarkably, using this method we observed only ~3% of the mono-and di-protected analogs combined. Still, by MALDI-MS we were seeing nearly 40% of the protected products from the same sample.

After numerous control experiments, including investigating the ionization efficiencies for all of the possible products and using an Orbi-Trap MS-MS to confirm sequences, we were able to confirm the validity of the LC-MS analysis.

Ultimately, we accepted the fickle-nature of MALDI-MS and again felt confident in our synthetic protocols for library development. Conformation of the attachment of the boronic acids proceeded with less uncertainty, relying on a previously identified binding assay with alizarin red S (ARS). In the end, we were able to identify other orthogonal amine protecting groups (i.e. MTT on long side-chain amines) that will simplify syntheses related to studies on poly-valency as well as for incorporating other side-chain functionality such as biotin. Using the Orbi-Trap MS we were also able to obtain better sensitivity and enhanced sequencing efficiency as compared to MALDI-MS.

Task 1 b): Screen peptide libraries with prostate cancer associated glycoproteins and complex glycans to identify highly selective and cross-reactive synthetic lectin (SL) hits. (Months 1-36)

The screening methods previously used to identify SL1-SL5 were employed to screen portions of our library against prostate cancer associated glycoproteins. As we continue to improve these screening methods we will continue to improve the quality of the hits we identify. Initially, we screened the library with ovalbumin (OVA) and porcine stomach mucin (PSM) as these glycoproteins contain glycans of interest that have been associated with prostate cancer (PCa), namely mannose and N-acetyl glucosamine (GlcNAc) on OVA and GlcNAc and fucose on PSM. From these screens, four new SLs were isolated and sequenced (SL6-SL9 in Table 2).

Beyond simply identifying new SLs, we have learned a great deal about how we do our analysis, specifically in how we image our resin and extract color data. In all of our image acquisition and analysis we have always been conscientious of the quality of the image and how we extract luminosity data. Still, until recently all decisions had been made by the user, which can introduce user bias. Therefore, in order to limit introduction of external bias we wrote a bead finding and data extraction algorithm using MATLAB. Of particular

Table 2. Sequences of identified SLs.

SL Hit	Sequence	Glycoprotein Screened	Glycoprotein Selectivity
SL1	Ac-RG**D***VTF**D***R-BBRM-resin	OVA	Cross reactive
SL2	Ac-RT**D***RFL**D***V-BBRM-resin	OVA	OVA
SL3	Ac-RS**D***VTT**D***R-BBRM-resin	OVA	OVA
SL4	Ac-RR**D***TQT**D***Q-BBRM-resin	PSM	OVA, PSM
SL5	Ac-RA**D***TRV**D***V-BBRM-resin	PSM	PSM
SL6	Ac-RT**D***NRN**D***F-BBRM-resin	PSM	OVA, BSM
SL7	Ac-RS**D***YFT**D***Q-BBRM-resin	PSM	OVA, PSM
SL8	Ac-RT**D***YGN**D***N-BBRM-resin	PSM	PSM
SL9	Ac-RT**D***YQV**D***A-BBRM-resin	PSM	OVA, PSM

interest to us was eliminating any inhomogeneity across the field of view, which could result from variation, between users, in the illumination source settings, focus or hardware alignment. The simplest approach was to define a region of interest (ROI) that could be set and used to reduce any edge effects. From there we could simply have the software "find" the beads based on relative intensity changes. In addition, we created the option to reject any identified objects based on size (area or circumference), circularity and/or pixel saturation at any given percentile of the pixels for each bead. Remarkably, reprocessing existing images with this algorithm, using only the ROI and rejection based on size, improved classification accuracy, based on leave-one-out methods, from 97% to 99% for 5 cell lines.

In the second year of funding we have continued to optimize our data acquisition, extraction and analysis protocols. In particular, an integral change was made to our MATLAB algorithm in order to improve the identification and quantification of individual assay beads. One challenge we continually face is how to extract data from dark images resulting from weak binding between an SL and a certain analyte, while still maintaining confidence in comparing these results with those from other SLs that bind more analyte and as a

result are much brighter. At the heart of this challenge is how to accurately find the edge of the dark bead compared to the background. Given that we typically carried out our analysis based on luminosity or brightness measurement we always found particles based on a fold-change over background using a greyscale image that resulted from merging the red, green and blue channels from our color camera. While the fold-change value can be readily changed to reduce the threshold, this often resulted in blurry edges and increased variability in our measurements. In the new MATLAB algorithm we have chosen to find the particles, i.e. identify the edges, using the color channel with the greatest amount of information, for example using the green channel for fluorescein and the red channel for rhodamine. Using this new design, we are able to reliably and consistently identify beads with intensities around 5 on an 8-bit scale, whereas the previous protocol limited us finding beads with intensities closer to 15 on an 8-bit scale.

Task 1 c): Upon identifying ≥5 hits, we will sequence, resynthesize, and determine the selectivity of identified hits towards the target that they were selected against as well as the other prostate cancer associated glycoproteins and complex glycans. (Months 3-36)

As described above, the four new hits listed in Table 1 were sequenced using MS-MS techniques and were resynthesized on TentaGel resin. To identify general selectivity trends, and for comparison with the original five SLs identified, each SL was bound with three glycoproteins (OVA, BSM, and PSM) as well as BSA, which was used as the control for nonspecific protein binding to the beads. Briefly, the library and the SLs were blocked with 1% BSA to minimize nonspecific binding, and then incubated with 0.1 mg/mL FITC-labeled analytes for 16 hours. After washing with PBS to remove unbound analyte, beads were imaged using a fluorescent microscope and color data extracted using the MATLAB algorithm described above. The library was used as a control, to reduce the differences between each glycoprotein in the extent of fluorescent labeling and degree of glycosylation. As such, the average raw intensity values for the library was subtracted from each replicate measure for each SL binding analyte. This normalized difference was then divided by the raw intensity of the library to afford a relative percent change for each SL binding each analyte. As shown in Figure 6, all of the SLs are cross-reactive to some degree. For example, while SL1 is considered completely cross-reactive, showing virtually no selectivity for any particular analyte, SL5 and SL6 display exquisite selectivity for PSM over BSM (~50-fold) and BSM over PSM (~60-fold), respectively, The remaining newly identified SLs show between 1.6 and 18-fold selectivity for one analyte over another.
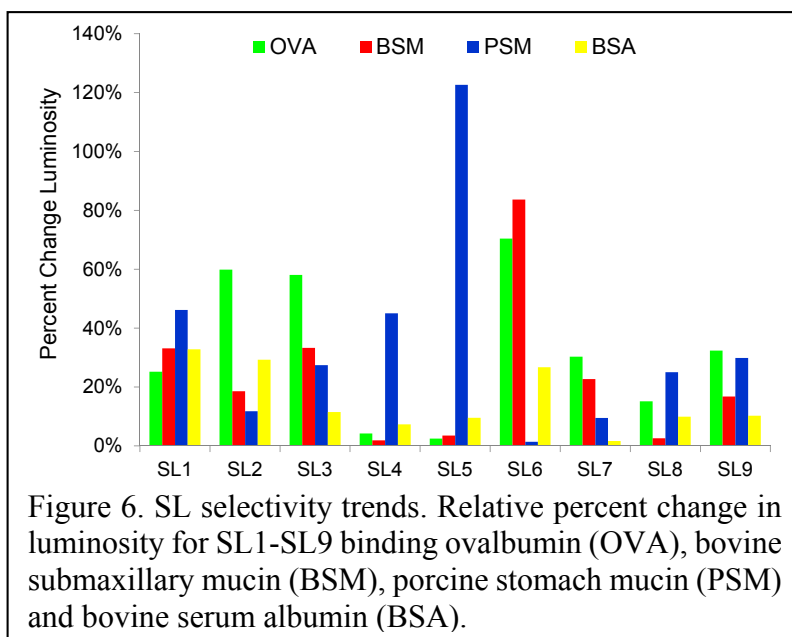

Figure 6. SL selectivity trends. Relative percent change in luminosity for SL1-SL9 binding ovalbumin (OVA), bovine submaxillary mucin (BSM), porcine stomach mucin (PSM) and bovine serum albumin (BSA).

While continuing to evaluate these hits throughout the second year of funding for this project, there is one theme that has become obvious. Most notably, the cross-reactive SLs that exhibit modest selectivity in this chicken-cow-pig paradigm (CCP, derived from ovalbumin (chicken), bovine mucin (cow) and porcine mucin (pig)) as indicated in Figure 3, typically provide the most useful information when assaying cancer related samples. In this same manner, generally speaking, the high selectivity that one can achieve for cow over pig mucin (e.g. SL5, 50-fold selectivity) does not translate into effective discriminatory capabilities within our SL Array. For example, when using a SL

Array composed of SL1-9 to evaluate the metastatic potential of six prostate derived cell lines (including: RWPE-1 (Healthy); WPE1-NA22 and WPE1-NB14 (cancerous non-metastatic); LNCAP, DU145 and PC-3 (cancerous metastatic), achieved with 100% accuracy) we see that 66% of the variance, or discriminatory ability of the array, is accounted for from SL2 and SL3, 25% and 41%, respectively. Recall that we previously excluded SL2 because of the similarities in response to purified glycoproteins with SL3 as well as noting the high BSA, background binding in SL2. Ultimately, the take-home lesson for us has been 1) that we cannot take any SL for granted, and 2) identifying SLs from more biologically relevant samples could provide better classification and more detailed information regarding the particular glycosylation patterns associated with a particular disease state.

Task 2. Initiating PI: Examine the biochemical/biophysical basis of the glycan•SL interaction. (Months 3-36)

Task 2 a): Upon identifying ≥5 hits (Task 1), we will develop a structure-activity relationship for highly selective SLs based on: 1) Alanine scanning 'mutagenesis'; 2) Varying the tether length; 3) Varying the boronic acid linkage and substitution patterns; and 4) Examining boronic acid substituent effects, to identify the factors that promote the selective recognition of a glycan by a particular SL. (Months 3-32)

While we have had previous success using 2-phenylboronic acid as our glycan targeting moiety, we also wanted to see if the recently described benzoboroxole would serve as a more suitable boronic acid. We first synthesized the carboxy-benzoboroxole (Figure 7A) and then coupled it to the same side-chain Dab amine on SL5 as was used for the PBA derivative. Interestingly, benzoboroxole-SL5 showed increased affinity for PSM when compared to the original PBA derivative (Figure 7B). Due to the improved affinity, we built both a peptide library (diversity = 11^5; 1.6 x10^5 members) as well as a peptoid library (diversity = 9^5; 5.9 x10^4 members) incorporating the benzoboroxole moiety. While we were able to successfully screen the peptide library and identify a hit ("Box1" - MRBB–VDARTDGR), sequencing the boroxole hits has been challenging due to the effect of the benzoboroxole moiety on ionization. As such, we are optimizing a variety of oxidation and cross coupling steps

Figure 7. Library design. **A.** Synthesis of carboxy benzoboroxole to conjugate to peptides/peptoids. **B.** Improvement of PSM binding to SL5 when using benzoboroxole instead of phenylboronic acid.

that we expect will efficiently remove the benzoboroxole functionality, and thereby facilitate the successful sequence of hits. Additional structure-activity relationships will be determined once we accumulate ≥5 hits.
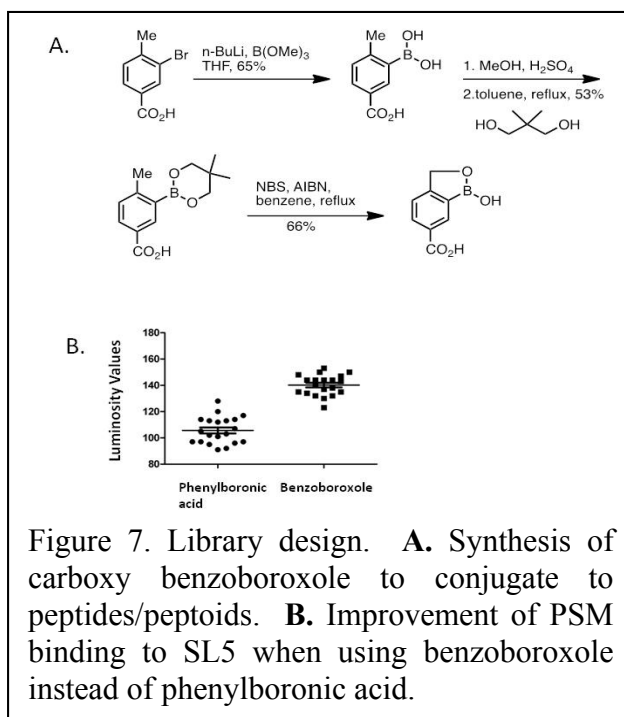
Task 2 b): Examine the contribution of multivalency towards binding affinity/selectivity of particular SLs. Synthesize mono-, di-, and tri-topic versions of the SLs identified in AIM 1 and evaluate their importance for glycan binding and selectivity. (Months 18-36).

To examine the effects of multivalency on SL affinity and selectivity we have begun to synthesize monovalent, two trivalent analogs varying the distance between the SL chains, and polyvalent SL5 based on poly(acrylic acid) (Figure 8). In our initial efforts, the mono and trivalent SL5 analogs are being synthesized on Rink-Amide resin using HBTU/Fmoc chemistry. The first amino acid attached to the resin was Fmoc-Cys(Mmt)-OH because the Mmt group can be removed orthogonally to other protecting groups used in the synthesis to install a reporter dye using thiol-selective maleimide chemistry (recall Cys is not used in the

12

library synthesis). For the monovalent SL5, Fmoc-Lys(ivDde)-OH was next coupled. The N-terminus was acylated, the side chain of lysine was deprotected with hydrazine and the desired SL synthesized using standard methods. Synthesis of the trivalent SL5 analogs begins like that of the monomeric derivative, however instead of acylating the N-terminus, the chain is extended with either one glycine or 3 glycine residues as spacers between the lysine branches that contain SL5 (Figure 8).
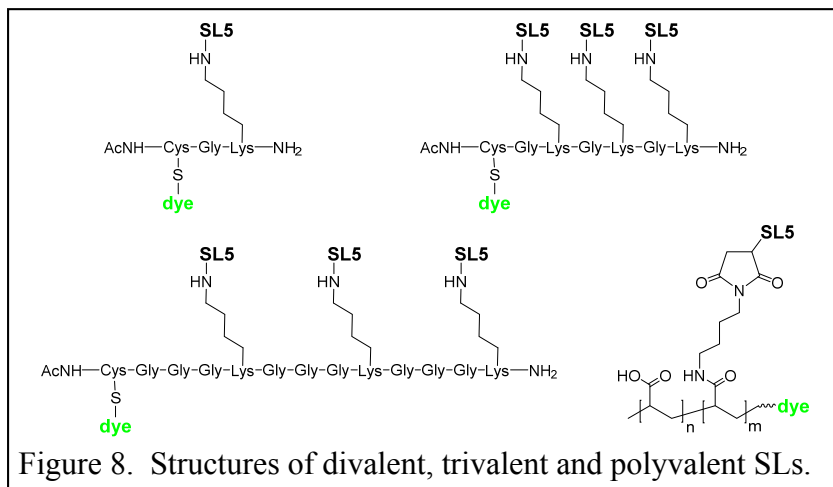

Figure 8. Structures of divalent, trivalent and polyvalent SLs.

Differing amounts of glycine can be incorporated between the Lys units to explore the effect of SL density on glycan binding. Sequential addition of Lys and glycine spacers provides the desired tri-topic scaffolds. Subsequently, the lysine side-chains are deprotected with hydrazine and the desired SL synthesized in triplicate using standard methods in parallel. After the Dab side-chains are deprotected using hydrazine and the boronic acids are coupled via reductive amination, the Mmt protecting group on Cys is removed using 1% TFA and the free thiol attached to a maleimide containing reporter tag (there is no interference with the boronic acid). To obtain additional information related to the intensity of the fluorescence signal upon binding, as well as to probe the structure-activity relationship related to functionalization of the SL termini, we have also attached fluorescent dyes to the terminal amine of the Gly-Lys scaffold as well as to the N-terminus of each SL. Finally, the SL analogs are cleaved from the resin with concurrent removal of the acid-labile side-chain protecting groups using 95% TFA.

With these synthetic steps completed we are currently working to purify and validate the structure of these SLs. Purification of the trivalent SL5 has proven to be a non-trivial task and we are having difficulty fully characterizing these novel structures. Consequently, we are proceeding to a higher order, more broadly defined polyvalent SL5 derived from commercially available poly(acrylic acid) (PAA). Modification of PAA begins with using EDC/HOBT to couple each acid side-chain with 1,4-diaminobutane. The resulting amine functionalized polymer is then partially derivatized with maleic anhydride to afford the maleimide modified PAA which can be coupled with our Cys-terminated monovalent SL5. Any remaining primary amines can be left to afford an overall positively charged polymer, acylated to provide a neutral polymer, reacted with succinic anhydride to obtain the anionic polymer or partially modified using any of these methods to tune the charge on the polymer backbone. We are just now beginning this synthesis and are excited about the opportunities available via this approach to vary in a controllable manner, the SL density and overall ensemble charge. Affinity and selectivity of each SL analog will be studied using a Fluorescence Polarization (FP) assay established in the PIs' labs and/or a microtiter plate-based approach relying on immobilization of the glycoprotein followed by "staining" with the labeled SL analog.

Task 2 c): Feed information from the above studies back into the library design process to aid the generation and subsequent identification of highly selective SLs. (Months 9-32).

Based on our experience with the benzoboroxole, which improved the affinity of SL5 for PSM, we are focused on incorporating this moiety into libraries once we optimize library sequencing. The lessons learned from the Partnering PI's structure-activity-relationships are also being incorporated into the design process (see below).

Task 3. _Partnering PI_: Examine the biochemical/biophysical basis of the glycan•SL interaction and develop SL-based sensor arrays for the proposed prostate cancer diagnostic. (Months 1-36)

Task 3 a): Develop a structure-activity relationship for previously identified SLs (SL2 and SL5) based on: 1) Alanine scanning 'mutagenesis'; 2) Varying the tether length; 3) Varying the boronic acid linkage and substitution patterns; and 4) Examining boronic acid substituent effects to identify the factors that promote the selective recognition of a glycan by a particular SL. (Months 1-12)

In our analysis of how structure impacts binding affinity and selectivity of SLs for glycoproteins, we have identified some expected and some unexpected correlations. These studies have largely revolved around SL2 and SL5 because they represent opposite ends of the spectrum; in that SL2 displayed modest selectivity (~2-fold) with high background binding while SL5 exhibited high, nearly 50-fold selectivity, with low non-specific binding. In selecting these two SLs we wanted to learn more about what factors most significantly impact binding for highly selective and modestly selective SLs to better understand if the same factors are important for each. In the end, we are focused on improving our approach towards generating new SLs capable of effectively discriminating between healthy and cancerous samples.

Using alanine scanning mutagenesis with SL2 for binding OVA (**_Task 3 a-1_**, Figure 9A) we see that charge on the peptide is important for binding affinity. Specifically, replacing R4 with alanine causes a 60% decrease in binding compared to native-SL2. Similarly, R1 and the arginine found in the C-terminal MRBB-sequence also reduce binding, though to a lesser extent (45% and 24% respectively). Likewise, binding affinity is reduced by more than 50% when the aminomethyl-phenyl boronic acids (D* = 3,7-Dab-2-PBA) are replaced with alanine or phenylalanine. However, when the Dab residues were left unmodified or alkylated with benzaldehyde, thereby leaving the charged ammonium at neutral pH, binding affinity was only diminished 2-3%. Similar trends were observed in SL5 for binding with PSM

Figure 9. Alanine scanning mutagenesis. **A.** Relative binding for SL2-mutants with OVA. **B.** Relative binding for SL5-mutants with PSM.

(Figure 9B). For example, when R5 was replaced by alanine binding was decreased nearly 55% and replacing both D* with alanine resulted in a 65% binding decrease. Interestingly, when T4 was replaced by alanine PSM binding was enhanced 25%. Similarly, when V6 or V8 was replaced with alanine a 20% and 5% increase in PSM binding was observed, respectively.
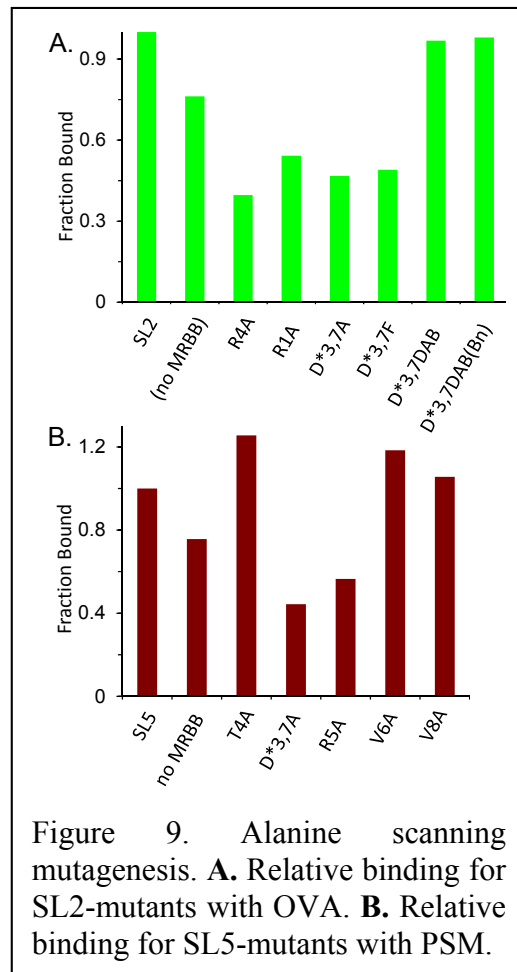
The role that the boronic acids play in defining SL binding affinity and selectivity was also studied (**_Task 3 a-3_**). In general, there was no observed loss of affinity when regio-isomeric phenyl boronic acids (PBAs) were used in SL2 and/or SL5, yet the PBA is undoubtedly important for defining selectivity (Figure 10). As seen in Figure 10A, there is no appreciable change in the selectivity patterns whether the boronic acid is _ortho-_, _meta-_ or _para-_ to the linkage to the peptide. This observation was unexpected 1) because of expected conformational preferences for sugar binding based on positioning the boronic acid in a specific orientation to bind the sugar, and 2) because when the boronic acid is _ortho-_ to the amino-methyl group enhanced diol binding is expected due to conformational and Lewis acidity trends. Still, binding between saccharides and _meta_-linked boronic acids has been observed particularly when involved in a polyvalent system, thereby

providing support for this observation. When the more sterically crowded and conformationally restricted 2-Ac-PBA is incorporated into SL2 the binding preference for OVA actually increases, though modestly (from 3-fold to ~6-fold). Most notably, however, is that when the PBA is replaced with a simple benzyl-group all selectivity is lost. SL5 showed similar trends (Figure 10B); with the orientation of the boronic acid having no significant influence on glycoprotein binding. Interestingly, in contrast to what was observed for SL2, the binding selectivity for SL5 decreased when the bulky 2-Ac-PBA was used, perhaps providing some insight into the steric and/or hydrophobic nature of the bound sugar environment. The final boronic acid modification, adding electron-donating ($-OCH_3$, $-NR_2$) and electron-withdrawing ($-CF_3$, $-NO_2$, $-CN$) substituents onto the PBA to alter the Lewis acidity of the boronic acid (**Task 3 a-4**), unquestionably showed no impact on analyte binding.

The length of the side-chain connecting the PBA to the peptide (i.e., the tether length, **Task 3 a-2**) was also
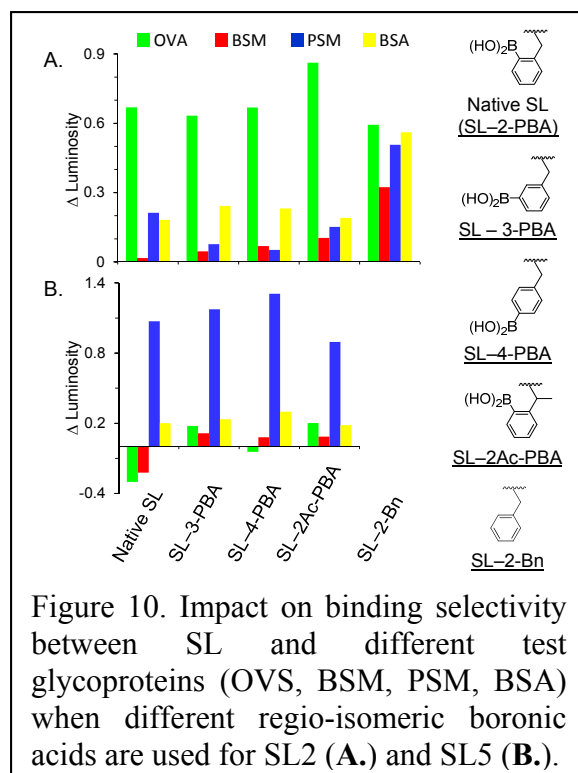

Figure 10. Impact on binding selectivity between SL and different test glycoproteins (OVS, BSM, PSM, BSA) when different regio-isomeric boronic acids are used for SL2 (**A.**) and SL5 (**B.**).
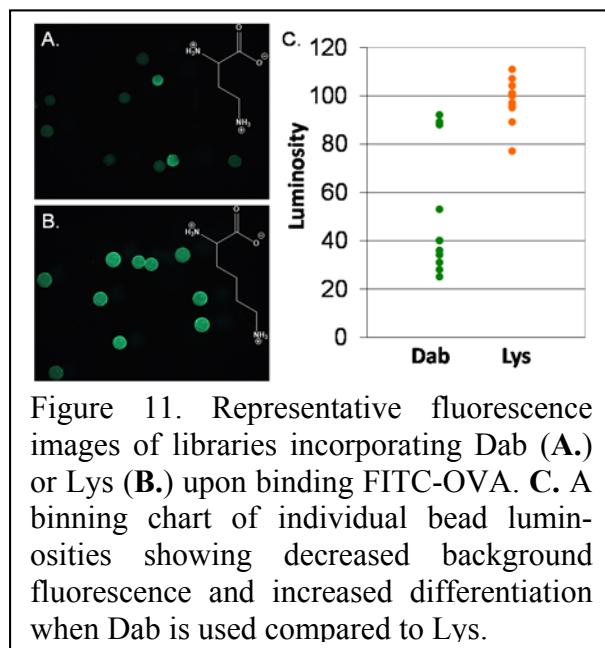
investigated. For this analysis, Dab and Lys were incorporated as the amino acid to which the boronic acid was attached in order to probe how degrees of freedom and thus preorganization can impact binding selectivity. Figure 11A and B show representative fluorescence images of portions of two libraries, derived independently from attachment of PBA to either DAB or LYS, after incubation with FITC-OVA. The Dab-based library displays decreased non-selective binding, as indicated by the decreased background fluorescence and increased library differentiation. Figure 11C is a binning chart, in which individual bead luminosities are plotted for each library. The greater spread in the data obtained for the Dab-containing library, versus the otherwise identical LYS-containing library, is an indication of greater differentiation and selectivity for binding the targeted glycoprotein.

As a final investigation of how structure can impact binding between SL and glycan, we looked at what impact the fluorescent label could have. SL1-SL5 are cationic, each containing a minimum of three arginine residues, and fluorescein is anionic at physiological pH. Based on what we learned about how charge impacts affinity in our alanine scanning mutagenesis studies, we wanted to determine how the dye charge was impacting binding affinity. We therefore labeled each of our glycoproteins with coumarin (as a neutral alternative) and rhodamine (as a cationic alternative) separately. If the charge on the dye significantly impacts the affinity of the SL for any given glycoprotein, we should see a decrease in the binding response as we move from fluorescein to coumarin, which is in fact what we observe (Figure 12). Still, rhodamine

Figure 11. Representative fluorescence images of libraries incorporating Dab (**A.**) or Lys (**B.**) upon binding FITC-OVA. **C.** A binning chart of individual bead luminosities showing decreased background fluorescence and increased differentiation when Dab is used compared to Lys.

labeled glycoproteins would be expected to have a further reduced binding affinity due to the cationic dye, which is contrary to our results. We conclude from this that our microscope filter set is somehow

inappropriate for the coumarin dye we are using, even though the wavelengths described seem relevant. Regardless, we are much more confident that labeling our targets is an appropriate method for identifying hits diagnostic.

Figure 12. Relative binding response for SL2-SL5 binding with PSM, labeled with coumarin (blue), fluorescein (green) or rhodamine (red).

Efforts to evaluate and understand the SL-glycan binding interaction have continued into the second year of funding while previous results have been fed back into our SL design. For example, based on the remarkable correlation between SL charge and binding affinity, we have made certain to include at least one arginine residue near each terminus of our SLs, while also taking a closer look at the importance of arginine residues near the middle of our SLs. It is clear that upon removal of any of the positively charged arginine residues from the basic SL5 sequence binding affinity is reduced (Figure 13). In initial studies (discussed above), the R5A mutant of SL5 showed nearly a 55% decrease in binding to PSM compared to the native SL5. In the present studies, we observe nearly a 40% decrease for the same mutant. Importantly, the trend remains the same, the small difference in these observed changes likely results from a change in glycoprotein concentration (0.5 mg/mL (old) to 0.1 mg/mL (new)). This reduction in analyte concentration was made to help reduce our hit rate so that we can focus on tighter binding SLs while also helping to reduce cost when using clinically relevant glycoproteins.

In further evaluating binding selectivity, alanine scanning mutagenesis was carried out to study SL2 and the mutants binding to proof-of-concept glycoproteins (BSA, BSM, OVA, PSM). Recall that previous studies only examined how these mutants bound to OVA. As indicated in Figure 14A, removal of any of the charged arginine residues (SL2-no MRBB, SL2-R4A, SL2-R1A) results in a loss of binding, though the relative binding pattern for the four glycoproteins remains virtually unchanged, with the exception of SL2-R4A where the BSM/PSM selectivity inverts. Similarly, removing the Dab and the PBA cause a decrease in binding affinity for all glycoproteins studied. Interestingly, for the SL2-D*3,7F mutant the binding selectivity is changed such that this SL prefers binding to FITC-BSA, even in the presence of 1%

Figure 13. SL5 mutant selectivity trends based on fraction bound compared with SL5 binding ovalbumin (OVA), bovine submaxillary mucin (BSM), porcine stomach mucin (PSM) and bovine serum albumin (BSA).

(w/w) BSA. Finally, upon reintroduction of the Dab residue as either the primary (SL2-Dab) or secondary amines (SL2-Bn), while still lacking the boronic acids, the overall affinity is recovered but the selectivity is dramatically reduced, indicating the importance of the charge on SL2 mutants in binding to (+5 in each of these mutants) but not necessarily in discrimination of these different glycoproteins.

Furthermore, we had previously shown that by shortening the amino acid side-chain, onto which the PBA is attached, from four methylenes (lysine) to two methylenes (Dab), we can reduce non-specific background binding to the boronic acids and thereby increase selectivity by taking advantage of pre-organization (Figure 11). We took this analysis one step further, moving from two to one methylene spacer between the peptide backbone and the PBA attachment point (Dab to Dpr (diaminopropanoic acid), respectively). Simultaneously, we evaluated the significance of the boronic acids on these SL5 and Dpr mutants. The first pattern, labeled
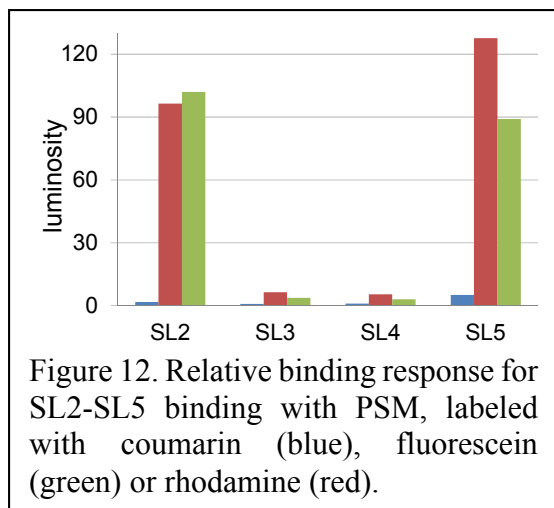
"SL5 raw," in Figure 14B simply shows the normalized response (by the greatest intensity) for SL5 responding to our four proof-of-concept glycoproteins. Note that even in this raw form, SL5 still binds most significantly with PSM. The second pattern, for SL5, shows the simple normalization (to one) of the response of SL5 binding to each glycoprotein (as a reference for comparison). Note that when the boronic acids are not included, as depicted for SL5-Dab, the affinity (indicated by reduced bar size) and selectivity (indicated by the pattern being the inverse of that for SL5 raw) displayed by SL5 is lost, providing additional evidence for the importance of the boronic acids in our approach. While we previously saw that SL2-Dab maintained high affinity for OVA even without the boronic acids (Figure 11), SL5-Dab does not follow this trend, even though both SL mutants are overall 5+ charged. This is not a surprising result because we expect that the boronic acids and the peptide sequence is more significant in defining the SL5 binding interactions than they are for SL2 based on the higher selectivity exhibited by SL5 compared to that of SL2.

We are also continuing to examine our analysis protocols that define the relative response of each SL for a series of different analytes. In the case of studying purified glycoproteins, we previously used the average response from 20 library beads as a reference. While this does provide a

Figure 14. A) Binding selectivity for SL2 and SL2-mutants, and B) raw binding intensities for SL5 and SL5 mutants all responding to OVA, BSM, PSM and BSA.

control set containing all of the potential cross-reactive elements that could interfere with our assessment of binding selectivity, it is also susceptible to large variations depending on sample size. If we were to use our entire library, this would be an ideal reference, however, new "reference libraries" would need to be synthesized and evaluated for each glycoprotein, each time new samples were made (to account for labeling variation) and this is not reasonable. As this method has been used, i.e. with small sample sets (n=20), the inclusion of one "hit" within the library "reference" data is sufficient to vary the average between 10-30% based on typical luminosity values for identifying a hit (e.g. assume average library background luminosity ~ 30 for n = 20; including one "modest hit" (luminosity ~100) changes this average to ~33 and including one good hit (luminosity ~200) changes the average to ~38; if n = 15 the range changes to 15-40% variability).

As a consequence of this variability, we have evaluated other means of accounting for instrument, user and labeling variability. As a first response, regular examination of the optical set-up using NIST-certified control particles (commercially available) ensures the consistency of our hardware set-up. We have also evaluated a number of "SL control sequences" to be used as reference controls, including: acylated resin, MRBB, octa-ala and SL5 (Figure 15). The acylated resin does not sufficiently bind with anything and consequently, when we image the beads after incubation with tagged analyte, we most often cannot even find the particles to measure. The MRBB and octa-ala sequences coat the resin particles with a peptide-based structure while
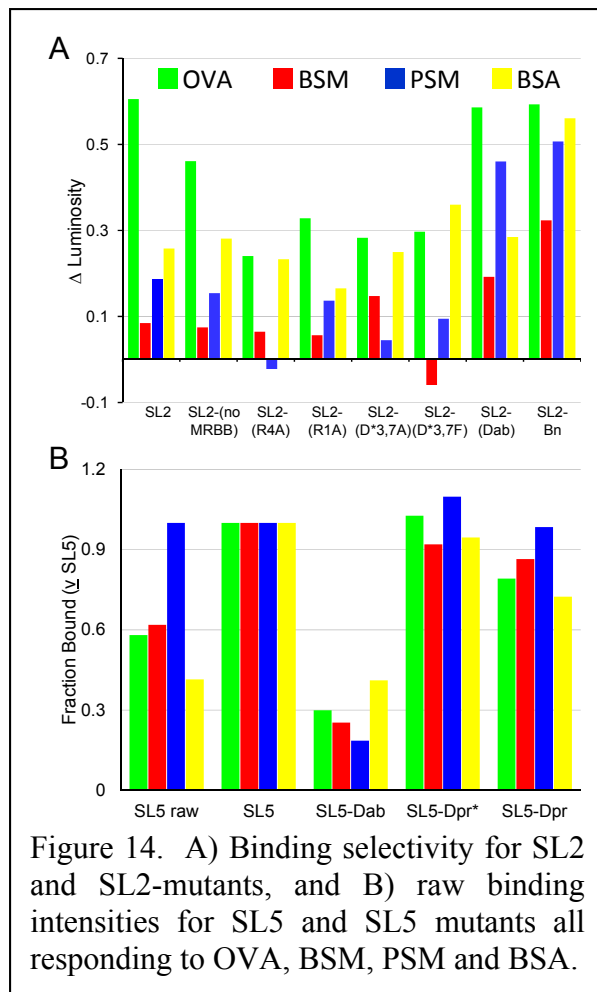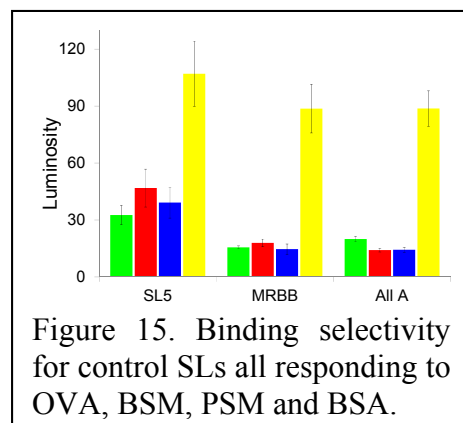

Figure 15. Binding selectivity for control SLs all responding to OVA, BSM, PSM and BSA.

offering little to no structure to afford discrimination of analytes beyond the inherent stickiness of the sample. Due to the similarity in the response from each of these models, we have focused primarily on the MRBB sequence. While the "look" of the SL binding pattern for each SL changes, the general trends are maintained. SL5 is an interesting option that we have used extensively, particularly as indicated in any of the figures in this document with a Y-axis label reading "Fraction Bound". Using an existing SL as a reference offers many benefits, perhaps most importantly is that it provides a known response pattern to standard glycoproteins that can be statistically evaluated to assess the differences and, by association, the similarities between runs (e.g. using MANOVA), subsequently producing a correction factor if needed. As a minor downside to this approach, the analytes which bind best to the SL, by definition, return the smallest response from the other SL Array members due to the mathematical approach (i.e. dividing by a large number). Nonetheless, we are continuing to evaluate these approaches and regardless of how we manipulate our raw data, the final analysis has been quite consistent.

With respect to the cell and tissue based work, we can simplify the analysis by normalizing the response from each SL responding to each different sample type (e.g. divide the response from each SL by the brightest measurement from all of the SLs responding to one cell line or tissue sample). This approach removes any labeling variability between samples of the same type as each preparation would be considered a unique sample at this point, while also addressing instrument variation (as long as samples are run at the same time) and user variability. Even with this simplified analysis we are still searching for the optimal reference method to most accurately address all of our sources of variability while preserving the integrity of the SL Array pattern and maximizing the SL Array response.

As a final element in these detailed investigations, we have just begun to investigate the impact of the dye charge and structure by changing from fluorescein and rhodamine to a pair of Alexaflour dyes (Figure 16). These Alexafluor dyes contain the common xanthene core like fluorescein and rhodamine. However, they both contain ammonium and sulfonate groups that promote water solubility and while also reducing the overall charge disparity that we see when comparing binding between our SLs and fluorescein and rhodamine labeled glycoproteins.

Figure 16. Molecular structures of Alexafluor 488 and Alexafluor 594.
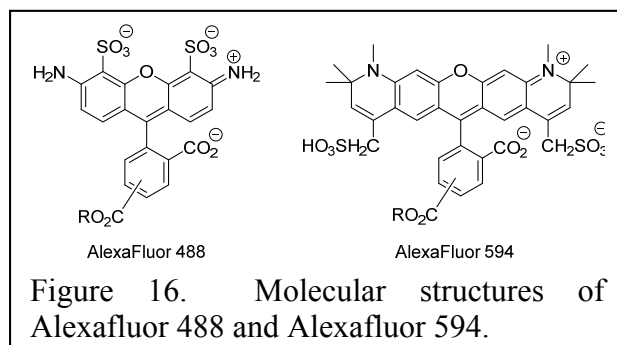
Task 3 b): Upon identifying ≥5 selective and cross-reactive SLs (Task 1), we will assemble them, and others identified in Task 2, into an array-based diagnostic format. (Months 1-36)

During the second year of funding on this project our main focus in this area has been to develop a more "user-friendly" platform for acquiring and analyzing our SL Array results. While using fluorescence microscopy has afforded excellent result, it is a labor intensive and time consuming process. Therefore, microtiter plate based assays were tested as a possible new array format. Two designs were studied. In the first, SLs biotinylated at the C-terminus were attached to neutravidin coated plates and fluorescein-labeled analytes were bound to the SLs on the plate. In the second approach ELISA plates were coated with unlabeled analyte and fluorescein-modified SLs were allowed to bind to the analyte immobilized in the plate wells. Either of these formats would have allowed for a plate-based fluorescence assay that could be read with any fluorescence plate reader.

In both cases SLs bound to the proof-of-concept glycoprotein analytes (BSA, BSM, OVA, PSM) and retained selectivity trends similar to those observed for SLs on beads. However, the affinity of the SLs for the analyte was markedly lower. As a result, very weak intensity readings were obtained that did not afford a large enough dynamic range to obtain intensity measurements from both strong and weak binders. Additionally, the variability within the assay was quite large (up to 50%) making pattern analysis nearly

impossible. Still, given the encouraging results obtained using simple monovalent SLs, we plan to revisit this concept again once we have polyvalent SLs available.

As we continue to evaluate alternate assay formats, we turned to a more high-throughput method of collecting and analyzing fluorescence data associated with SL-glycoprotein binding, namely flow cytometry, as a means to read out the fluorescence intensity derived from labeled analytes binding with resin-bound SLs. This approach has the added benefit of allowing SL synthesis and glycoprotein binding to be carried out on beads, thereby maintaining our desired polyvalency and the resulting binding characteristics of the beads. Briefly, synthesis of SLs followed the same procedure as described above differing only in that 10μm mono-disperse TentaGel beads were used to adhere to the particle size limits for analysis on the available Flow Cytometer (BD LSR II). SLs synthesized on these beads had binding profiles similar to those synthesized on larger 300μm beads as assessed using flow cytometry (Figure 17).

Evaluation of cell membrane extracts has focused on colon and prostate derived cell lines. Four human colon cell lines

Figure 17. Comparison of the binding selectivity for SL1, 3, 4 and 5 to four glycoproteins OVA, BSM, PSM and BSA when data is collected by A) Microscopy or B) Flow Cytometry.

were chosen for analysis; CCD 841 CoN (Healthy); HCT116 and HT29 (cancerous non-metastatic); LOVO (Cancerous metastatic). SL1-9 were bound individually to fluorescein-labeled cell membrane extracts. Unbound protein was washed away and beads were passed through a BD LSR II flow cytometer. Individual intensity readings were recorded for each bead within a sample, extraction of this type of data resulted in the ability to acquire intensity values from hundreds of beads. Outliers were rejected at 1.8 interquartile distances (IQDs) and intensity readings were normalized to one using the brightest reading for each cell line. To complement existing colon cancer data, Linear Discriminant Analysis (LDA) was carried out and classification accuracies determined for discrimination between healthy, cancerous non-metastatic and cancerous metastatic cell lines based on leave-one-out cross-validation. Compared to 93% classification accuracy obtained for data acquired from microscope images of large beads, the classification accuracy from flow cytometry data was only 73%.

Focusing on prostate derived cell lines, six human prostate cell lines were analyzed; RWPE-1 (healthy); WPE1-NA22 and WPE1-NB14 (cancerous non-metastatic); LNCAP, DU145 and PC-3 (cancerous metastatic). Based on LDA of flow cytometry data prostate cancer cell lines classified with 81% accuracy (Figure 18) compared to 100% from microscope images for this three class model. When simply comparing healthy or cancerous samples, using flow cytometry, our SL Array predicts sample type with 97% accuracy. In comparison to microscope-based collection of data and analysis, this method allows a comprehensive and

Figure 18. 2D LDA plot of flow cytometry data from the SL Array responding to six prostate cancer cell lines, classified with 81% accuracy.

unbiased approach. While these results are indeed exceptional for this type of analysis, the outcomes are obviously not as robust as the microscopy-based analysis and progress needs to be made if this design is to
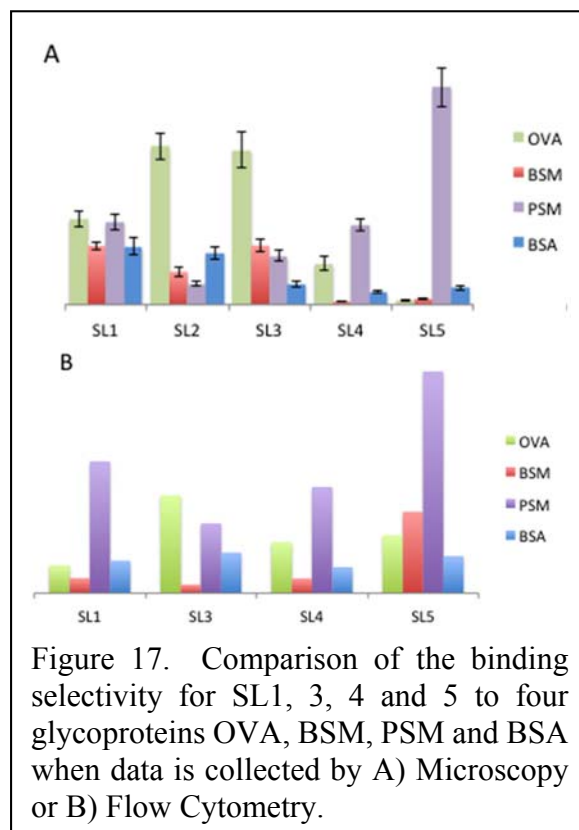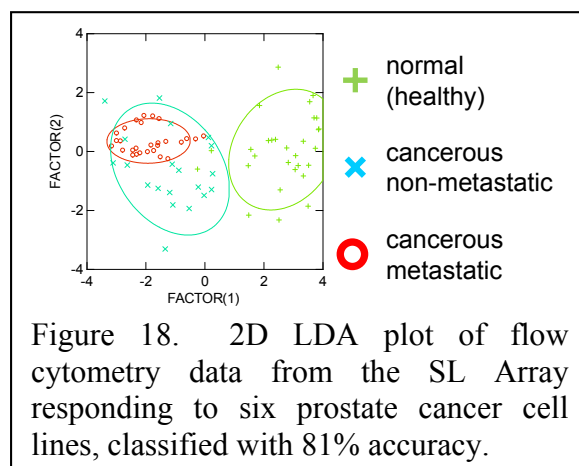
compete. One area to be worked on more is in how we apply boundaries to our raw data. The sheer amount of data obtained from using flow cytometry can be overwhelming and more detailed analysis of the quality of these data sets needs to be carried out.

While we continue to improve the efficacy of our SL Array we are also looking to enhance not only the user interface (as described above) but to also expand the assay utility by working with clinically relevant and less invasively collected samples (**Task 3 d** includes a discussion of using our SL Array to assess human tissue samples based on metastatic potential). In an effort to move towards serum-based analysis, we have begun to study the secreted glycoproteins found in the media from cultured cell lines. Four human colon cell lines were chosen for analysis; CCD 841 CoN (Healthy); HCT116 and HT29 (cancerous non-metastatic); LOVO (Cancerous metastatic). We have therefore taken secreted glycoproteins isolated from cell culture media as well as membrane extracts from the cells taken from the exact same media. Furthermore, we have evaluated our SL Array response towards media containing fetal bovine serum (FBS) as well as starving the cells of FBS for 48 hours prior to harvesting the secreted and membrane glycoproteins. Briefly, membrane extracts were isolated and labeled with FITC as previously described. Cell culture media containing the secreted glycoproteins was concentrated using ultra centrifugation. The secreted proteins were then precipitated into acetone, centrifuged, and the supernatant removed. The pellet was washed once with acetone and the previous step repeated. The cell pellets were re-suspended in buffer and labeled with FITC without any further purification.

Figure 19 shows the 2D plot of the LDA results from the analysis of secreted (Figure 19A) and membrane extracts (Figure 19B) for each of these four human colon cell lines, using SL1-9 binding to fluorescein labeled glycoproteins to generate response patterns. Notice that in each plot, the data clusters into three groups (normal/healthy, cancerous non-metastatic, cancerous metastatic) with virtually no overlap. Cross-validation of each model indicates classification accuracies of 100% for the secreted and 96% for the membrane extracted glycoproteins. Most excitingly, when these two sets of data are combined and modeled together (Figure 19C) we see excellent overlap, with an overall classification accuracy of 92%; suggesting that there is a high correlation between the amounts and types of glycoproteins secreted and those integral to the cell membrane. In addition, whether we starve the cells of FBS or not, even with all of the different bovine proteins and

Figure 19. 2D LDA plot of microscope-obtained data from the SL Array (i.e. SL1-9) responding to secreted (**A**) and membrane extracted glycoproteins (**B**) from four human colon cell lines; with classification accuracies of 100% and 96% respectively. **C**) LDA plot obtained from modeling data from the secreted and membrane extracted glycoproteins together, achieving 92% classification accuracy.

glycoproteins present in the sample, makes little difference in the statistical analysis. All of this taken together provides further support for the use of our SL Array to assess secreted glycoproteins from clinical samples.
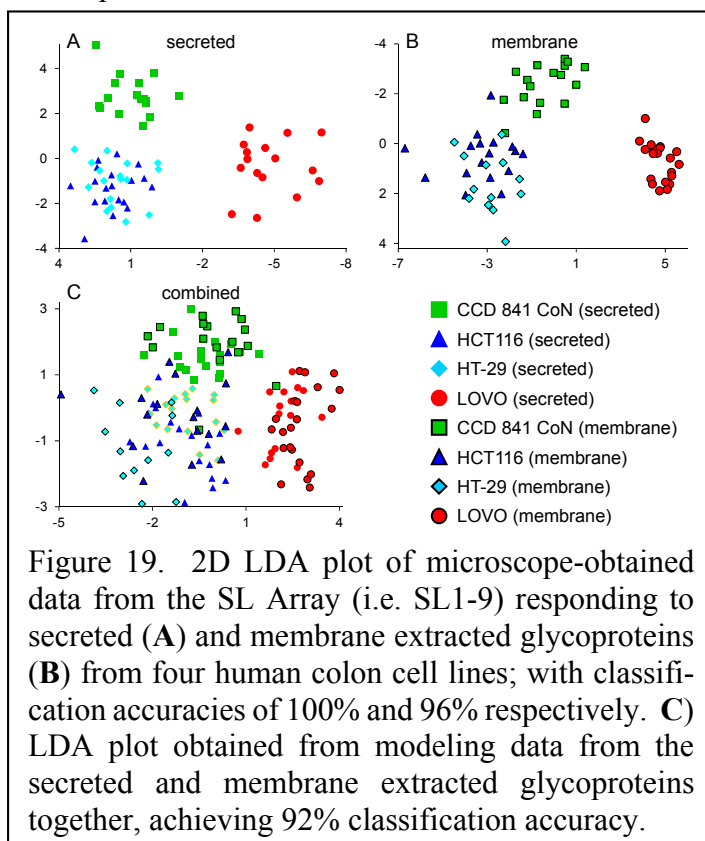
Task 3 c): Evaluate the ability of the array to discriminate complex glycans (i.e., TF antigen, Le^a, Le^x, sLe^a, sLe^x). Note that because the development of the arrays will be continually evolving, as we identify new and more selective SLs, the time frame for this task is the entire proposal period. (Months 1-36)

As an initial test of our approach towards binding biologically relevant targets, we used an array of SL1, SL3, SL4 and SL5 to distinguish between five structurally similar cancer associated glycans (TF antigen, Le^a, Le^x, sLe^a and sLe^x; Figure 2A). These glycans were chosen because they represent some of the more common saccharide motifs overexpressed by cancerous cells as well as being composed of many of the same monosaccharides that were found on our proof-of-concept glycoproteins (OVE, PSM, BSM). SL2 was not included in the array based on the assumption that we could eliminate redundancy due to response similarities with SL3 and because of the high background binding to BSA as compared with SL3. Briefly, after incubating each SL with a solution containing biotinylated glycan and fluorescently labeled streptavidin, luminosity values, from fluorescence microscope images, were analyzed (4 SLs by 5 glycans by 15 replicates). To account for differences in bead size and loading levels, luminosities were normalized against the highest luminosity within a given SL type (in this study the greatest degree of variability stems from bead-to-bead variations). The unique pattern generated for each different glycan based on the response of the four different SLs is shown in Figure 20A. Note that the response for each glycan produces unique and distinguishable patterns that are reproducible within the limits of the associated error.

To interpret patterns that display subtle differences, statistical analyses were used to identify the most significant features necessary for classification of the analytes, specifically, linear discriminant analysis (LDA). From this analysis, Discriminant 1 and Discriminant 2 contain 83.3% and 14.8% of the between group variation, respectively (Figure 20B). Note that the different glycans are clustered into five groups with an average standard deviation of 6%. Furthermore, the Wilks' lambda value for this analysis is 0.009 with a p-tail value of <0.000001, indicating that there is a statistically significant difference in the population means from this analysis at the 95% level of confidence. Based on leave-one-out cross-validation the SL array correctly classified 71 of the 75 measured samples (94.7% classification accuracy, with a chance accuracy of only 20%). Significantly, the Lewis antigens and their sialylated forms (Le^a/Le^x and sLe^a/sLe^x) were efficiently discriminated while only differing by the addition of a terminal sialic acid moiety.

Figure 20. Differentiation of 5 glycans using a SL-array. **A.)** Fingerprint pattern of the average normalized luminosity intensities from SL1, SL3, SL4, and SL5 responding to 5 different glycans (TF, Le^a, Le^x, sLe^a and sLe^x). **B.)** The 2-dimensional LDA score plot derived from the patterns shown in (**A.**) for 15 replicates. Ellipses indicate 95% confidence level, analyte identification indicated in the legends above.

Additionally, this SL-Array impressively distinguished between Le^a and Le^x, as well as between sLe^a and sLe^x, glycans where the only structural difference is the regiochemistry of the linkage to the core GlcNAc moiety (Figure 2A). Of the four misclassified glycans, Le^a was twice identified as sLe^a, sLe^a was once classified as Le^a, and Le^x was once recognized as sLe^a.

To further validate the utility of our SL Array for discriminating these five structurally similar glycans, the more statistically robust ''boot-strapping'' approach was used. Fifty separate and unique data sets were
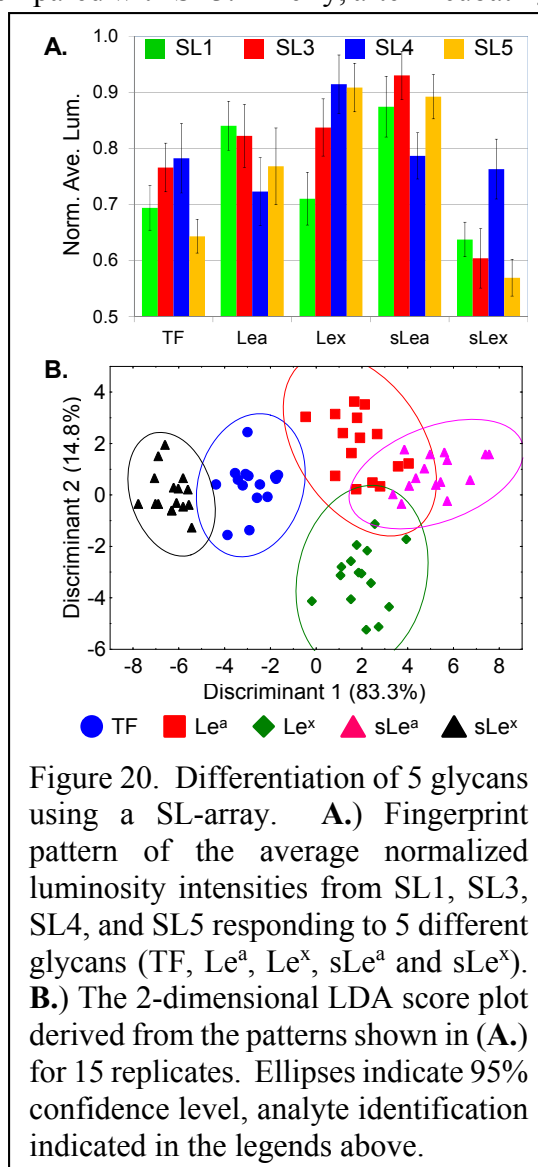
generated using the Mersenne–Twister random number generator. Overall, this analysis yielded 94% classification accuracy correctly classifying individual glycans from 86–99%. As with the leave-one-out analysis, the three greatest misclassifications were due to Le^a being misclassified as sLe^a (9.3%), sLe^a being misclassified as Le^a (6.7%), and Le^x being misclassified as sLe^a (4.7%). Still further stressing the limits of this array for differentiating glycans, training and test sets were chosen at random from the Normal distribution, splitting our data in half. One half was used as a training set, to create a statistical model, and the other half as a test set to assess the ability of this model to accurately identify these ''unknowns.'' Random set generation and subsequent analyses were carried out 25 times to create replicates in order to minimize systematic error. Consistent with the previously described analyses, the overall classification accuracy of this approach was 94%. The consistency displayed across the three methods further testifies to the strength of the outlined SL Array design for discriminating structurally similar cancer associated glycans.

As indicated above, it is possible that the SLs interact, not only with the glycan, but also with the protein portion of glycoproteins. In this analysis the protein component, FITC-streptavidin, is the same for each glycan being analyzed. As such, any observed difference in the response from the array must be attributed to the glycan constituent. Given the structural similarities between these glycans, it is remarkable that there were not more misclassifications. In total, these results validate our ability to differentiate structurally similar cancer associated glycans with high accuracy using a small, cross-reactive SL Array.

Task 3 d): Evaluate the ability of the array to discriminate prostate cancer cell lines (i.e. PC-3, LNCaP, and DU145), as well as RWPE-1, WPE1-NA22, WPE1-NB14, WPE1-NB11, and WPE1-NB26, which are referred to as the MNU cell lines, all available from the ATCC. Note that because the development of the arrays will be continually evolving, as we identify new and more selective SLs, the time frame for this task is the entire proposal period. (Months 1-36)

The vast majority of our work to date in developing and working with arrays has focused on how we analyze our array data. As described above, we have improved our data collection methods to obtain better consistency between replicate measurements as well as optimizing how intensity values are extracted.

In this regard, we have begun to evaluate our array response using color space intensities and not just luminosity. In particular we have focused on the popular "Red-Green-Blue" (RGB) color space to obtain more of a full spectral response from our array. In so doing we have improved our classification accuracy from 97% to 100% for a five cell line panel (including: HT-29, CT-26, CT-26-F1, CT-26-FL3, and 3T3/NIH) made up of 114 replicates we often use to evaluate our models.

To further validate our approach we have assessed the ability of our array to identify analytes which it has never seen before. Specifically, we used ten cell lines including a mix of mouse and human lines as well as colon (7 - 3T3, HT29, HCT116, CT26, CT26-F1, CT26-FL3, and Lovo), breast (2 - MCF7 and MCF10A) and prostate (1 - PC3) cell lines. To do this we create a statistical model based on 9 cell lines while leaving data from one cell line out and then attempt to classify this excluded line, in much the same way that a diagnostic test must determine the disease status for a patient that did not contribute to the calibration data set. As such, when classifying our samples as healthy, cancerous/non-metastatic or cancerous/metastatic we only obtained 56% overall classification accuracy (Figure 21, blue).

Figure 21. Individual classification accuracies (3-class groupings in blue, 2-class groupings in green) for each of 10 cell lines derived from a model lacking all input from that line.

However, if we simply look to diagnose the cancer and not stage it at the same time, thereby identifying our data as either healthy or cancerous, we improve our overall classification accuracy to just over 83%
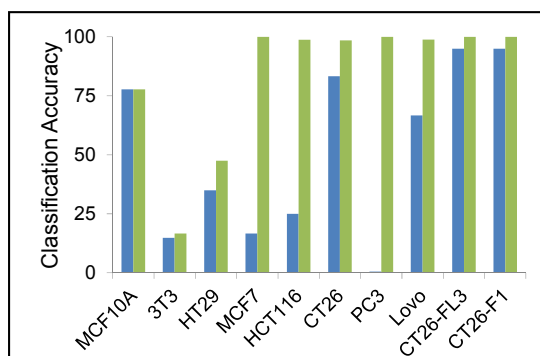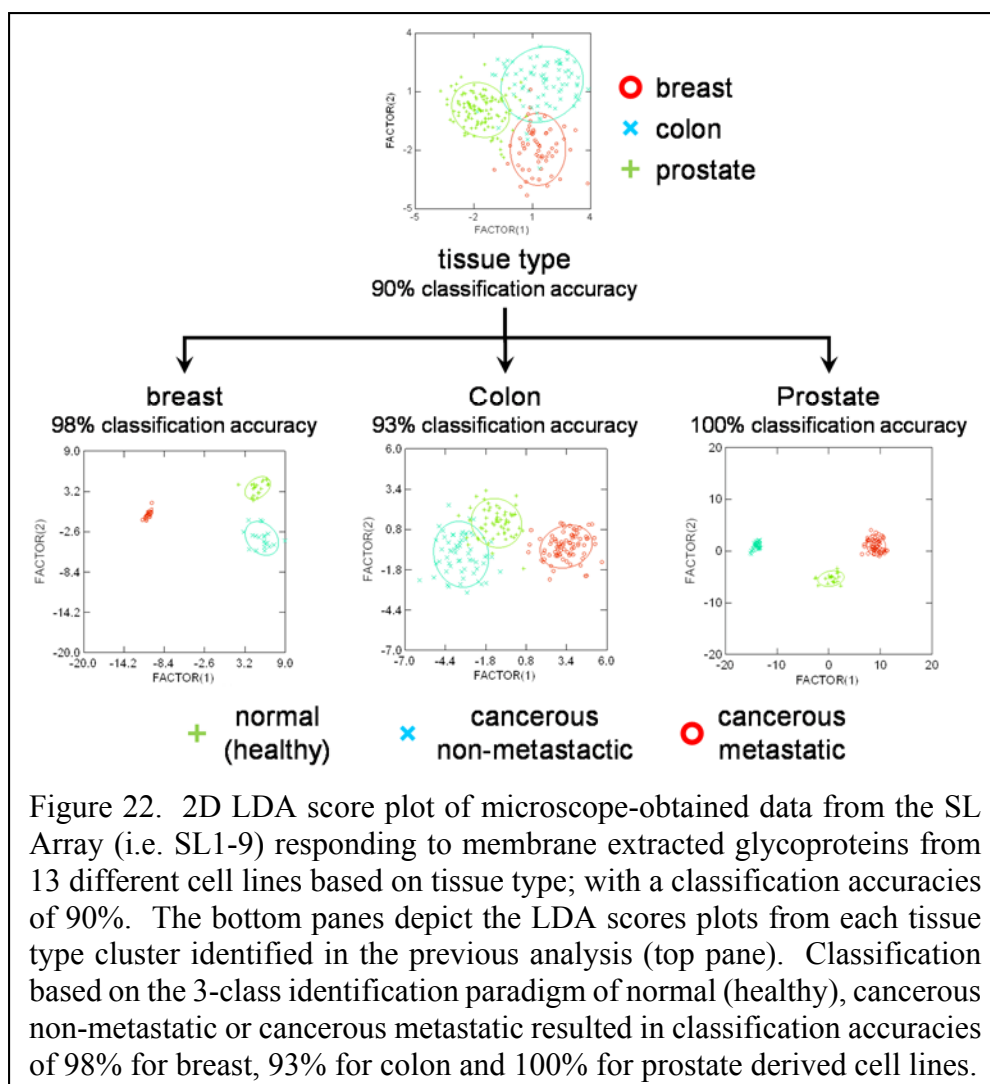
22

(Figure 21, green). Still, by ignoring the 3T3/NIH mouse fibroblast line, the most out of place cell line in this analysis, and looking at the remaining nine cell lines using this same approach, we can "diagnose" the presence of cancer 100% of the time, with a sample set of n = 434.

Finally, we realize that using linear discriminant analysis (LDA) is not necessarily the best approach for analyzing our data. We also recognize that not all samples can be controlled as tightly as ours have been previously. As such we evaluated our complete data set derived from colon cancer cell lines, including variations in incubation time (1 h to 24 h), incubation temperature (4 °C, 25 °C and 37 °C), and sample dilution (20x, 50x and 100x). In total this afforded nearly 12,000 measurements leading to 3000 different fingerprints from our SL Array. Using support vector machines we were able to obtain 93% classification accuracy and using regression tree analysis we improved the classification accuracy to 97%. Working closely with Prof. Edsel Pena in the Department of Statistics at the University of South Carolina we are continuing to explore our options, being cautious that the approach we take is appropriate for the type of analysis we are doing as well as verifying that we do not "over-train" our models and that we maintain statistical validity.

As part of our focus during the second year of funding on this project we aimed to expand our previous work, which focused primarily on colon cancer related cell lines, to include prostate cancer related samples as well. Furthermore, existing data analyses from ten colon cancer cell lines using our SL Array relied heavily on murine cell lines (nearly half); and we desired to focus this aspect of our analyses on human derived cell lines only. Therefore we expanded our analysis to include 15 human cell lines consisting of four colon derived cell lines (HCT 116, LoVo, HT-29, CCD 841 CoN), five breast derived cell lines (MCF10A, MCF7, MDA-MB-231, BT474, D47T) and six prostate derived cell lines (LNCaP, DU145, PC3, RWPE-1, WPE1-NA22, WPE1-NB14). Initially, a healthy human colon cell line was tested in place of NIH 3T3s, a murine fibroblast cell line, as part of a colon cancer model for determining metastatic potential. The addition of the human normal colon cell line (CCD 841 CoN) in place of a mouse cell line (NIH 3T3) improved overall classification accuracies. Known tissue specific differences in glycosylation led to the addition of tissue-specific normal cell lines, specifically, RWPE-1, a healthy prostate cell line.

Figure 22. 2D LDA score plot of microscope-obtained data from the SL Array (i.e. SL1-9) responding to membrane extracted glycoproteins from 13 different cell lines based on tissue type; with a classification accuracies of 90%. The bottom panes depict the LDA scores plots from each tissue type cluster identified in the previous analysis (top pane). Classification based on the 3-class identification paradigm of normal (healthy), cancerous non-metastatic or cancerous metastatic resulted in classification accuracies of 98% for breast, 93% for colon and 100% for prostate derived cell lines.

When examining data from all cell lines, the removal of murine-based cell line data as well as the increase in the number of human cell line data resulted in the ability to classify cell lines as healthy vs. cancerous with 79% accuracy. A significant improvement was seen when classifying samples as healthy, cancerous/non-metastatic or cancerous/metastatic for the human only cell lines with a classification accuracy of 76%, as compared to the model which included the murine cell line data, having a classification accuracy of only 56%.

However, since tissue specific differences in glycosylation have been shown to occur, we evaluated the ability of our array to distinguish these cell lines based on tissue type. The top pane in Figure 22 shows the two-dimensional data spread from using LDA to analyze 13 different cell lines based on tissue type (four colon derived cell lines (HCT 116, LoVo, HT-29, CCD 841 CoN), three breast derived cell lines (MCF10A, MCF7, MDA-MB-231) and six prostate derived cell lines (RWPE-1, WPE1-NA22, WPE1-NB14, LNCAP, DU145, PC-3), achieving 90% classification accuracy based on leave-one-out cross-validation. Using LDA, this same type of analysis, was run on each tissue type cluster identified in the previous classification process to evaluate these subsets for differing metastatic potential. Independently, each tissue type classified excellently, 98% for breast, 93% for colon and 100% for prostate based on the 3-class identification paradigm of normal (healthy), cancerous non-metastatic or cancerous metastatic. Overall, this afforded between 84% to 90% classification accuracy, compared to 76% when not including tissue type in the analysis.

Based on our particular interest in prostate cancer, we looked more closely at the data from only the prostate-derived cell lines. Briefly, the RWPE-1 cell line is also the parent cell line to a series of cell lines transformed by exposure to N-methyl-N-nitrosourea (MNU). These cell lines are representative of a progression from normal cells to cancerous/metastatic cells. To the best of our knowledge there are no low-/non-metastatic prostate cancer cell lines isolated from patient tissue which are commercially available. Therefore, of the four original NMU cell lines WPE1-NA22 and WPE1-NB14 were first analyzed as part of our prostate cancer model to assess metastatic potential because these are the closest to healthy, and thus representative of cancerous non-metastatic cells.

Using LDA we were able to show that our SL Array can distinguish between healthy (RWPE-1), cancerous/non-metastatic (WPE1-NA22, WPE1-NB14) and cancerous/metastatic cell lines (LNCAP, DU145, PC-3) with 100% accuracy (Figure 23). Here, we see that there is an obvious trend in the clustering based on metastatic potential regardless of cell line. For example, and perhaps not so surprising given that they are isogenic cell lines, the WPE1-NA22 and WPE1-NB14 cluster tightly together (red squares and green triangles, Figure 23); however, note that the RWPE-1 parent cell line (blue diamonds, Figure 23) are clearly separated from these tumorigenic cell lines. More notable is how the data from the LNCAP, DU145 and PC-3

Figure 23. 2D LDA score plot of microscope-obtained data from the SL Array (i.e. SL1-9) responding to membrane extracted glycoproteins from 4 prostate derived cell lines; distinguishing normal/healthy (RWPE-1), cancerous non-metastatic (WPE1-NA22 and WPE1-NB14) and cancerous metastatic (LNCAP, DU145 and PC-3) groups of cell lines with 100% accuracy.

cell lines cluster together (purple X, turquoise asterisks and orange circles, Figure 23), thereby indicating strong similarities in the glycosylation patterns of these more aggressive cell lines, overall suggesting a high correlation between array response and metastatic potential.

In addition to increasing the number of cell lines used as analytes the number of SLs used as part of the array has also been increased. SL2 and SLs 6-9 were initially discounted as part of an array due to low selectivity or repetition of selectivity. However, since tissue specific differences in glycosylation have been
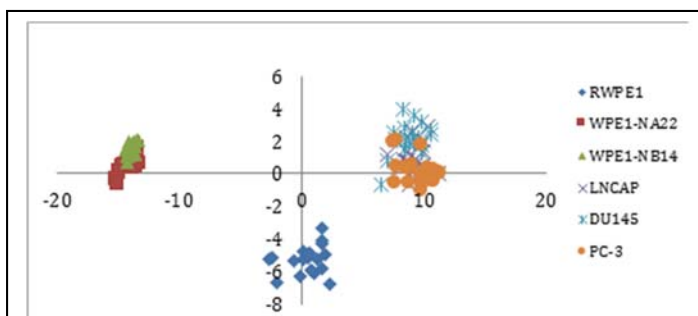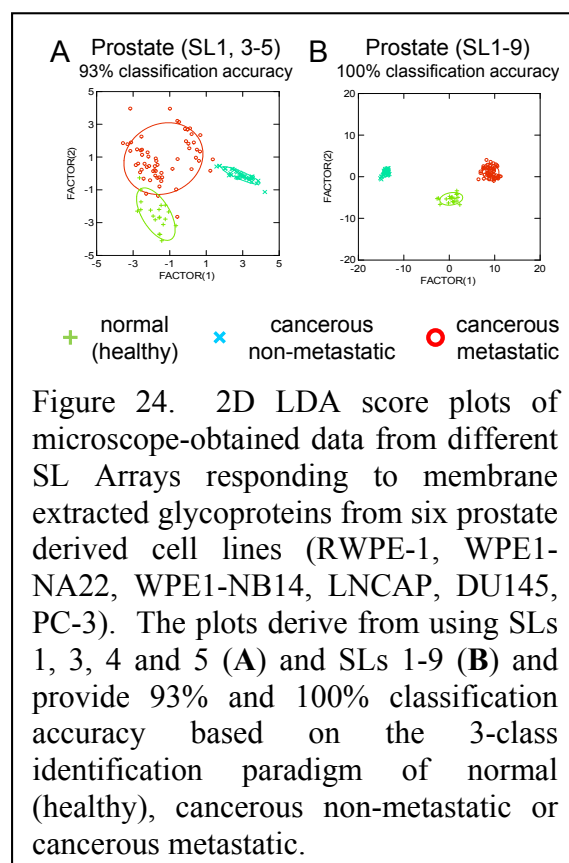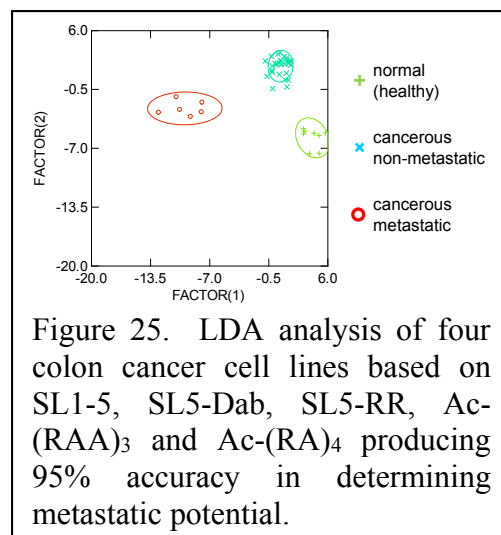
shown to occur, all SLs were included in the SL Array to determine if they provided greater accuracy in determining the metastatic potential of prostate cancer. When our original SL Array, including SL1, 3, 4 and 5, was used to evaluate the six prostate cancer cell lines based on metastatic potential, the array was able to distinguish between healthy, cancerous non-metastatic and cancerous metastatic cell lines with 93% accuracy (Figure 24A). When the same cell lines are assessed using the nine membered SL Array (SLs 1-9) the accuracy increases to 100% (Figure 24B). This suggest that while the individual SLs binding selectivity's may not be greatly different with respect to OVA, BSM and/or PSM, the inclusion of these differential binding SLs in the array provides incremental information for discriminating cell lines of differing metastatic potential. For example and as described above, SL2 was previously excluded from our SL Array because of the similarities in response with SL3 to purified glycoproteins as well as noting the high BSA, background binding in SL2; still in the current analysis, SL2 accounted for 25% of the variance in the array that could discriminate prostate derived cell lines with 100% accuracy (i.e. 25% of the discriminatory ability of the array was provided by SL2).

Figure 24. 2D LDA score plots of microscope-obtained data from different SL Arrays responding to membrane extracted glycoproteins from six prostate derived cell lines (RWPE-1, WPE1-NA22, WPE1-NB14, LNCAP, DU145, PC-3). The plots derive from using SLs 1, 3, 4 and 5 (**A**) and SLs 1-9 (**B**) and provide 93% and 100% classification accuracy based on the 3-class identification paradigm of normal (healthy), cancerous non-metastatic or cancerous metastatic.

In addition, array diversity was expanded by including the charged arginine mutants discussed **Task 3 a**. In evaluating the same four human colon derived cell lines, using SL1-5 along with SL5-Dab, SL5-RR, Ac-(RAA)₃ and Ac-(RA)₄ in different combinations provided classification accuracies between 95%-100% (Figure 25). While using SL1-9 consistently produced 100% classification for this group of cell lines, it is interesting to note that SL4, SL5-Dab and SL5-RR accounted for nearly 81% of the diversity captured by this array, suggesting charge is important in certain analyses and adding to our array capabilities.

While the current array discriminates cell lines with classification accuracies continuing to improve by refining the SLs in the array and improved statistical modeling, this is not our ultimate goal. Cell lines do serve as acceptable *in vitro* models for cancer, however they do not always represent the complexity of the tumor microenvironment. To examine whether our SL Array could work with clinical specimens, tissue from 11 colon cancer patients were analyzed using the SL Array containing SL1-9. This tissue was readily available from the Colon Cancer Research Centre Tissue Biorepository, which JJL is a member. Each patient tissue sample consisted of one tumor sample and one normal or healthy sample taken from an adjacent site.

Briefly, the tissues were ground in liquid nitrogen and the resulting powder added to lysis buffer. Membrane proteins were extracted using the Qiagen membrane extraction kit, labeled with FITC and incubated with SLs1-9. Fluorescence intensity data was collected for each sample using fluorescence microscopy. Outliers were rejected at 1.8 interquartile distances (IQDs) and intensity readings were normalized to one using the brightest

Figure 25. LDA analysis of four colon cancer cell lines based on SL1-5, SL5-Dab, SL5-RR, Ac-(RAA)₃ and Ac-(RA)₄ producing 95% accuracy in determining metastatic potential.

reading for each patient sample. Using de-identified patient disease data, LDA analysis was carried out to determine the ability of the array to differentiate patient samples based on a number of factors. Of greatest importance was the ability of the array to tell the difference between healthy and cancerous tissues and to accurately stage the cancer. Using this nine SL array we were able to distinguish healthy and cancerous samples with 83% accuracy and stage the cancer with 91% accuracy. Most interestingly, we were able to identify patients who had pre-adjuvant chemotherapy prior to surgery as the "normal/healthy" tissue samples from these patients more closely resembled tumor tissue samples than they did normal/healthy tissue from patients who had not yet received any chemotherapy. These initial results demonstrate that our array not only discriminates between cell types effectively in *in vitro* cell line models but also in tissue samples. This represents promising data suggesting that development of the array for clinical utility is possible. The next set of pressing experiments is to evaluate tissue samples from prostate cancer patients and to follow-up with serum samples from similar patients.

Finally, on a different but quite exciting note, we have been able to classify triple negative breast cancer (TNBC) using our SL Array with high accuracy. Since we have demonstrated the ability of our SL Array to distinguish between tissue types and classify cell lines and tissue samples based on metastatic potential; it is of interest to determine if the SL Array can be used to distinguish between different molecular subtypes of cancer. The basis of our current research using our SL Array is that during the progression of cancer, from healthy to cancerous/metastatic, glycosylation profiles change. One of the best-characterized cancers in terms of molecular subtypes is breast cancer. It can be broken down into four broad subtypes, Human Epidermal growth factor Receptor 2 (HER2) overexpressing, Luminal A, Luminal B and Triple Negative, based on the expression levels of three receptors; HER2, Estrogen Receptor (ER) and the Progesterone Receptor (PR). Therefore, SLs 1-9 were used in an array format to determine if we could classify five breast cancer cell lines into these molecular subtypes based on the SL-glycan interactions. In brief summary, from this analysis (based on SLs1-9 and evaluated using LDA), we were able to distinguish these four subtypes with 98% accuracy. Given the lack of known markers for TNBC, these results are quite exciting! Furthermore, the ability of our SL Array to distinguish between well characterized subtypes of breast cancer suggests that it may be of use in this capacity for other types of cancers, for example in determining androgen sensitivity in prostate cancer.

Key Research Accomplishments (Year 1)

- **Synthesized peptoid libraries (PRT).** Peptoid based SL libraries (diversity = 9^5; 5.9 $\times 10^4$ members) were synthesized on Tentagel macro beads and their utility for identifying SL's targeting proof-of-concept glycoproteins assessed. The library was also used to further optimize our screening procedures. Screening with this library to identify selective SL's is ongoing. We are also moving toward the synthesis of β-amino acid containing libraries, which are intrinsically structured/pre-organized, we expect to further aid the identification of SL's with improved selectivity.

- **Synthesized peptide libraries (JJL and PRT).** Peptide based SL libraries (diversity = 11^5; 1.6 $\times 10^5$ members) were synthesized on Tentagel macro beads and also used to further optimize our screening procedures and identify several new selective SLs (see below).

- **Optimization of screening protocols (PRT).** The above libraries were used to identify optimized conditions for identifying SLs that selectively bind our proof-of-concept glycoproteins and CAGs. These conditions are: 10 mM HEPES, 150 mM NaCl, 0.1% E. coli lysate (stock conc. 8 mg/mL) and 0.05% TWEEN.

- **Developed a structure activity relationship (JJL).** Used SL2 and SL5 to develop a structure activity relationship. The key findings were that positive charge and the boronic acid are critical for affinity and selectivity. This information is being fed back into the library design process to aid in the generation and subsequent identification of highly selective SL's (see Tasks 2c and 3a).

- **Identified boroxole as a high affinity sugar binding motif (PRT).** The 2-formylphenyl boronic acid moiety was replaced with several different boronic acids to explore boronic acid substituent effects, and thereby identify the factors that promote the selective recognition of a glycan by a particular SL. The key findings were that the substitution pattern did not matter and that substituent effects (e.g. electron donating/withdrawing group) were minimal. Also, the boroxole moiety was identified as an alternative moiety with improved affinity.

- **Optimization of image capture and analysis (JJL).** A Matlab algorithm was successfully developed to automate data extraction from microscope images of our bead-based assays. The algorithm not only identifies each bead and extracts color space intensity values, but also allows for data rejection based on customizable threshold values for size, circularity and/or color space percentile high values (i.e., relating pixel saturation). Using this automated data collection system, additional statistical analyses have been performed on our colon cancer data sets, and using quadratic discriminant analysis and/or support vector machines, our classification accuracies improved from 97% to >99%.

- **Identified 4 additional SLs that bind proof-of-concept glycoproteins (JJL and PRT).** Screens of peptide libraries containing either 2-formylphenyl boronic acid or boroxole identified 4 additional SLs that bind proof-of-concept glycoproteins.

- **Identified SLs that selectively bind sialyl Lewis X over Lewis X, sialyl Lewis A, and Lewis A (PRT).** Screens of peptide libraries versus biotinylated-sialyl Lewis X identified two SLs (SLex1 and SLex2). Confirmation assays demonstrated that SLex2 selectively binds sialyl Lewis X over Lewis X, sialyl Lewis A, and Lewis A.

- **Used existing SL array to demonstrate the utility in diagnosing and staging prostate, breast, and colon cancer (JJL).** Using our SL array to classify various colon cancer cell lines according to metastatic potential, we achieved 97% classification accuracy as reported in our *Chem Sci* manuscript. Inclusion of additional colon, breast and prostate cancer cell lines (n = 10; 426 separate measurements), and grouping the different cell lines according to whether they are healthy, cancerous and cancerous/metastatic we achieve 84% classification accuracy. However, if we look at it from a diagnostic perspective, i.e. cancerous versus non-cancerous, the classification accuracy improves to 95%.

Key Research Accomplishments (Year 2)

- **Developed a Dual Dye screening protocol.** A method was developed to screen the fixed-position-library with mixtures of fluorescein and rhodamine labeled analytes. In one case, a fluorescein labeled membrane extract from the RWPE-1 cell line (normal) was combined with a rhodamine labeled membrane extract from the PC3 cell line (cancerous-metastatic), and this mixture was incubated with our SL library. Hits were identified as beads that were bright in one channel or the other (i.e., red or green) but not in both; thereby affording cross-reactivity between prostate and cancerous prostate markers.

- **Identified 5 additional SLs that bind prostate cancer related glycoproteins.** Screens of the fixed-position-library with FITC-PSA and labeled membrane extracts from RWPE-1 and PC3 cell lines identified 5 additional SLs that bind prostate cancer related glycoproteins.

- **Identified SL sequencing methods based on Edman Degradation.** Previous efforts to use Edman degradation methods had failed due to randomized boronic acid location and linker length (e.g. Lys, Orn, Dab, Dpr). Partial hydrolysis of the peptide backbone was observed after cleavage of the boronic acid moiety with peroxide, further complicating the Edman-based analysis. However with a fixed location and only one linker for our boronic acid, we have been able to use Edman methods to sequence our SLs with high fidelity, without removing the boronic acid group.

- **Optimized image analysis protocol.** A change was made to our MATLAB algorithm to improve the identification and quantification of individual assay beads from weak binding between an SL and a certain analyte (i.e. from dark images). The basic challenge was how to accurately find the edge of the dark bead compared to the background. In the new MATLAB algorithm the particles are found using the color channel with the greatest amount of information (e.g. the green channel for fluorescein), thereby improving the reliability and consistency of identifying beads with intensities as low as 5 on an 8-bit scale.

- **Developed a better understanding of the importance of cross-reactivity.** Notably, the cross-reactive SLs that exhibit modest selectivity in our proof-of-concept paradigm (ovalbumin, bovine mucin and porcine mucin) consistently provide the most useful information when assaying cancer related samples. For example, SL2 and SL3 account for 66% of the variance, or discriminatory ability of the array, when discriminating six prostate derived cell lines; yet SL2 and SL3 were cross-reactive, displaying no more than a 2-fold selectivity for any of the proof-of-concept glycoproteins.

- **Developed a structure activity relationship.** Continuing studies to evaluate the relationship between SL structure and glycoprotein binding affinity/selectivity, and thus diagnostic prospect, have highlighted the importance of positive charge on the SL. Specifically, a combination of boronic acid functionalized SLs and highly positively charged SLs lacking boronic acids was used to discriminate colon cancer related cell lines with great effectiveness, in some cases better than when only SLs containing boronic acids was used. This information is being fed back into our design to improve the detection and staging capabilities of our SL Array by providing additional and still different information on the cell line in general.

- **Advanced SL Array design and utility to address clinical challenges.** Using flow cytometry to evaluate SLs (10μm beads) we have demonstrated the utility of our initial SL Array to mimic results obtained using more tedious and time-consuming fluorescence microscopy. Using Linear Discriminant Analysis (LDA), classification accuracies were determined for six prostate derived cell lines, discriminating healthy, cancerous non-metastatic and cancerous metastatic; providing 81% accuracy (microscope data was 100%). However, when simply comparing samples as healthy or cancerous using flow cytometry our SL Array predicted sample class with 97% accuracy. Additionally, moving towards serum-based testing, we have shown that samples secreted into culture media show the same response to our SL Array as those from membrane extracts. Finally, evaluation of human tissue samples match trends observed from cell lines.

- **Used SL Array to demonstrate diagnostic and staging utility in prostate, breast, and colon cancers.** Using LDA to interpret the results from an expanded SL Array, including SL1-9, we evaluated 15 human cell lines consisting of four colon derived cell lines (HCT 116, LoVo, HT-29, CCD 841 CoN), five breast derived cell lines (MCF10A, MCF7, MDA-MB-231, BT474, D47T) and six prostate derived cell lines (LNCaP, DU145, PC3, RWPE-1, WPE1-NA22, WPE1-NB14), obtaining 76% classification accuracy based solely on cancerous or normal. However, when we included the tissue source (breast, colon or prostate) into our analysis the overall classification accuracy improved, depending on the tissue type, to between 84% and 90%.

Conclusions

Significant progress has been made in the first two years of funding on this project to develop synthetic lectin (SL) arrays that bind to prostate cancer associated glycans and glycoproteins (CAGs) to detect glycosylation patterns associated with cancer. These studies are being pursued to develop this methodology into a robust system, thereby providing a new paradigm that can diagnose and stage prostate cancer. Moreover, these studies directly relate to the "Imaging," and "Biomarker" focus areas of the PCRP overarching challenges. In particular, the progress made towards creating a cross-reactive sensor platform will allow for more reliable diagnosis of prostate cancer and thus improve the likelihood of accurate detection and aid in managing prostate cancer, thereby decreasing many of the negative impacts associated with prostate cancer.

In year one, peptide and peptoid libraries have been synthesized and screened against cancer associated analytes. Consequently, six new synthetic lectins have been identified targeting both glycans (2 new SLs) and glycoproteins (4 new SLs). In so doing, we have been able to improve our methods for binding SLs to CAGs to reduce background binding, thereby improving our signal to noise ratio. We have also been able to advance our approaches to 1) acquire assay images, 2) extract assay response values and 3) analyze the assay outcome. Ultimately, these improvements have allowed us to verify the validity of our approach while also improving the overall assay accuracy. As such, we have enlarged our data set to nearly 12,000 measurements while expanding the assay relevance and at the same time maintaining classification accuracies between 93-97%. These results reflect assay responses to a combination of prostate, colon and breast cancer cell lines.

In addition to enhancing the overall assay performance, we have also advanced our understanding of what factors are important for SLs to bind CAGs. Specifically, we have demonstrated that boroxoles are efficient replacements for the originally proposed boronic acids and can improve the binding affinity of SLs for certain CAGs. We have also begun to develop a detailed structure-activity-relationship that has to date indicated that charge on the SL is important for defining binding affinity with CAGs while the boronic acids significantly contribute to binding selectivity.

In year two, new protocols have been developed to screen our SL libraries based on competitive binding between differently labeled glycoproteins or cell membrane extracts. Subsequently, five hits have been isolated and sequenced that unambiguously target prostate cancer associated glycoproteins. While developing these novel screening methods we have also been able to improve our sequencing and image analysis techniques. In particular, we can now effectively use Edman degradation schemes to sequence our SLs without having to remove our boronic acid groups. Regarding image analysis, we are now better able to identify our particle edges from fluorescence microscopy while also transitioning to flow cytometry based methods to afford higher throughput and more consistent data acquisition.

In evaluating how SL structure impacts binding affinity and selectivity with glycoproteins, we have gained a better understanding of cross-reactive SLs contribute to the overall SL Array effectiveness while also learning a great deal about how the charge and boronic acid group of our SLs impact binding and ultimately influence the utility of our SL Array for diagnosing and staging prostate cancer. As such, we have been able to expand the scope of our SL Array analysis to include breast, colon and prostate derived cell lines. We have also utilized samples obtained from cell-culture media that include secreted glycoproteins towards evaluating patient serum. Similarly, we have demonstrated that our SL Array can effectively discriminate human colon tissue samples.

As this project progresses, we will continue to expand our understanding of the factors important for SLs to bind CAGs. Specifically, we will study in greater detail how our SLs are interacting with clinically relevant targets. Ultimately, while initial studies have provided valuable insight into what factors contribute to SL-Glycan

binding, it is clear that what makes a good binder for PSM is not necessarily what is needed to make a good sensor for detecting prostate cancer, for example.In regards to screening the SL library and using these SLs in discerning normal and cancerous cell lines, we have importantly learned: 1) that we cannot take any SL for granted, and 2) identifying SLs from more biologically relevant samples could provide better classification and more detailed information regarding the particular glycosylation patterns associated with a particular disease state. As novel and exciting approaches, we will endeavor to incorporate fluorescent boronic acids into our SL design thereby eliminating the need to label our samples because the boronic acids change intensity upon diol binding. Furthermore, we plan to evaluate using our SLs to capture or stain glycoproteins as part of a spot array. Significantly, we are continually screening our libraries for new hits that better target prostate cancer and subsequently these hits are included into our array and used to better discriminate prostate cancer cell lines while simultaneously improving our signaling strategies, our data analysis and the overall utility of our approach.

Despite being located at two different sites JJL at USC and PRT moving from TSRI to the University of Massachusetts Medical School, the project has continued to grow and evolve through constant email and phone contact, as well as organized weekly meetings and scheduled site visits. As revealed above, each PI has contributed to different aspects of this project; with both PIs having overlapping and supporting roles for the other. Clearly, this team works well together, providing their own expertise to result in a level of productivity that is greater than that achievable by each PI working independently. Certainly, this project would not exist without the input of both PIs.

Publications, Abstracts, and Presentations

- Lavigne presented an invited seminar at the Southeast Regional Meeting of the American Chemical Society in Atlanta, GA in November 2013.
- Lavigne presented a seminar in the Department of Chemical Engineering at Texas A&M University in College Station, TX in May 2013.

Inventions, Patents and Licenses

- Nothing to report.

Reportable Outcomes (Year 1)

- Published a manuscript in Chemical Sciences[3] (see Appendices) detailing the utility of SL arrays to discriminate cancer cell lines based on metastatic potential, thereby setting the stage for further developing this approach for the diagnosis and staging of cancer.
- Kevin Bicker, who played a key role in developing the SL array, will begin his tenure track faculty position at Middle Tennessee State University in August 2013.
- Lavigne presented a seminar to the College of Pharmacy at the Medical University of South Carolina.
- Held joint lab meeting at The Scripps Research Institute, Scripps Florida, on July 25, 2013. Anna Veldkamp, Kathleen O'Connell, and Daniel Lewallen presented seminars on their SL studies.

Reportable Outcomes (Year 2)

- Jing Sun, who played a key role in developing the SL array, began his full-time Instructor position at Georgia Southern University in August 2013.
- Developed SL Array prototype as a research tool that can contribute towards the understanding, diagnosis, prognosis, and potentially treatment of a prostate cancer, ultimately working to improve patient quality of life.

Other Achievements

- Lavigne spent one week as a Visiting Scientist in the Department of Chemical Engineering at Texas A&M University in College Station, TX in May 2013.
- Lavigne and O'Connell (post-doctoral fellow) participated in the Space, Cancer and Personalized Medicine Conference at the Gibbs Cancer Center and Research Institute in Spartanburg, SC in May 2014.

References

(1) Liu, X., Dix, M., Speers, A. E., Bachovchin, D. A., Zuhl, A. M., Cravatt, B. F., and Kodadek, T. J. (2012) Rapid development of a potent photo-triggered inhibitor of the serine hydrolase RBBP9, *Chembiochem 13*, 2082-2093.

(2) Bicker, K. L., Sun, J., Lavigne, J. J., and Thompson, P. R. (2011) Boronic acid functionalized peptidyl synthetic lectins: combinatorial library design, peptide sequencing, and selective glycoprotein recognition, *ACS Comb Sci 13*, 232-243.

(3) Bicker, K. L., Sun, J., Harrell, M., Zhang, Y., Pena, M. M., Thompson, P. R., and Lavigne, J. J. (2012) Synthetic lectin arrays for the detection and discrimination of cancer associated glycans and cell lines, *Chemical Science 3*, 1147-1156.

Appendix A

Bicker, K. L.; Sun, J.; Harrell, M.; Zhang, Y.; Pena, M. M.; Thompson, P. R.; Lavigne, J. J. Synthetic Lectin Arrays for the Detection and Discrimination of Cancer Associated Glycans and Cell Lines. *Chem. Sci.* **2012**, *3*, 1147-1156. DOI: 10.1039/C2SC00790H.

EDGE ARTICLE

Synthetic lectin arrays for the detection and discrimination of cancer associated glycans and cell lines†

Kevin L. Bicker,[ab] Jing Sun,[a] Morgan Harrell,[a] Yu Zhang,[c] Maria M. Pena,[c] Paul R. Thompson[*b] and John J. Lavigne[*a]

Aberrant glycosylation is a hallmark of various disease states, including cancer, and effective detection and discrimination between healthy and diseased cells is an important challenge for the diagnosis and treatment of many diseases. Here, we describe the use of boronic acid functionalized synthetic lectins (SLs) in an array format for the differentiation of structurally similar cancer associated glycans and cancer cell lines; discrimination is based on subtle variations in glycosylation patterns. We further demonstrate the utility of our SLs in recognizing glycoproteins with up to 50-fold selectivity, even in 95% human serum. Given their robust and selective nature, these SLs were able to effectively distinguish (a) five structurally similar glycans with 94% accuracy; (b) seven normal, cancerous and metastatic colon cancer cell lines, including three isogenic cell lines, with 92% accuracy; and (c) these same seven cell lines using a guided statistical analysis to improve our analysis to 97% accuracy. In total, these data suggest that an SL-based array will be useful for the diagnosis of cancer.

Introduction

The intracellular and extracellular biomarkers displayed by healthy and diseased cells provide unique signatures by which these cells can be distinguished. For example, in healthy cells, post-translational glycosylation of proteins plays a critical role in cell–cell interactions and in cell signaling.[1] However, aberrant protein glycosylation is a hallmark of numerous diseases including inflammation and cancer, thus providing a means for the detection and classification of healthy and diseased states. Related to cancer, distinguishing between healthy and cancer cells that possess either low or high metastatic potentials typically relies on detecting subtle variations in the types and levels of specific biomarkers (*e.g.*, DNA, RNA, and proteins) using high-affinity, target-selective sensors, *e.g.* antibodies. Regardless of the analyte, these approaches all require prior knowledge of the markers targeted and no specific biomarker or combination of biomarkers has been identified to sufficiently differentiate between healthy, cancerous/non-metastatic and cancerous/

aDepartment of Chemistry & Biochemistry, University of South Carolina, 631 Sumter Street, Columbia, SC, USA 29208. E-mail: JLavigne@chem. sc.edu; Fax: +(803)-777-9521; Tel: +(803)-777-5264

bDepartment of Chemistry, The Scripps Research Institute, Scripps Florida, 120 Scripps Way, Jupiter, Florida, USA 33458. E-mail: PThompson@scripps.edu; Fax: +(561)-228-3050; Tel: +(561)-228-2860

cDepartment of Biological Sciences, University of South Carolina, 715 Sumter Street, Columbia, SC USA 29208

† Electronic supplementary information (ESI) available: Complete methods including: labeling, membrane extraction and screening protocols, Supplementary Figures S1–S5 and LDA classification data. See DOI: 10.1039/c2sc00790h

metastatic cell types. An alternative to this "lock-and-key" approach[2–6] would be to use cross-reactive recognition elements as part of a sensor array.

Cross-reactive sensor arrays incorporate multiple receptors with different affinities such that each component has a selective and unique interaction with the targeted analyte(s). As a result, the response from the entire array produces a fingerprint pattern characteristic of the analyte to which it is responding. That is to say that classification is not based on the response from a single receptor, but rather it is the composite response from the entire array that allows for identification and classification of the analyte. This practice has often been referred to as the "electronic nose" approach,[7–13] though, in this case, used for solution-based analysis.

While natural lectins (sugar binding proteins) display cross-reactivity, and lectin arrays can often offer an effective approach to cancer diagnostics, the methodology is often complex and the constituents are of inherently low stability and high cost.[14–17] Here we describe an alternate approach based on the covalent yet reversible binding between boronic acid functionalized synthetic lectins (SLs) and cancer associated glycans and glycoproteins. This design does not require previous knowledge of the biomarkers targeted; rather it is focused on identifying changes in glycosylation patterns, a factor that is known to play a significant role in oncogenesis and metastasis.

In cancerous cells, the expression of specific glycan structures can be increased, decreased, or even newly expressed. These changes often co-opt cellular signaling pathways to promote growth, division and metastasis.[1] For example, sialyl Lewis X (sLe^x) and sialyl Lewis A (sLe^a) (Fig. 1A) are overexpressed in
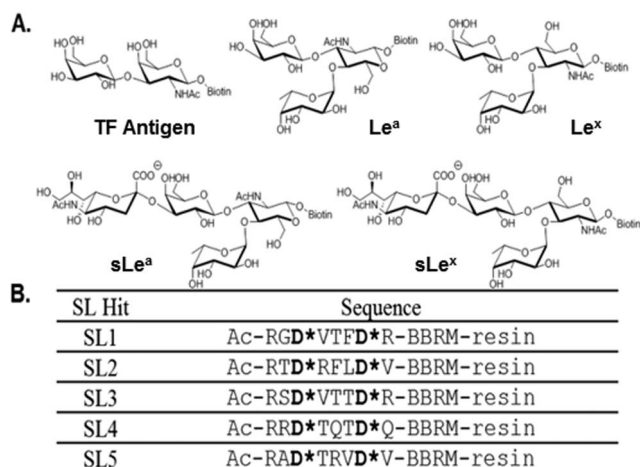
Fig. 1 (A) The structures of biotinylated cancer associated glycans used in this study. (B) The sequences of the SLs used for validation studies and in the array assessments.

breast, colon and pancreatic cancers,[1] and the increased expression of sLe[x] is known to enhance tumor metastasis.[18–21] Tests to detect specific aberrant glycosylation events are used for both initial disease diagnosis and monitoring disease progression yet suffer from limitations including a high number of false positives and a reliance on inherently unstable and costly antibodies or natural lectins.[14–17] For example, elevated levels of CEA (carcinoembryonic antigen), an aberrantly glycosylated glycoprotein, are associated with an increased risk of colon cancer relapse and metastasis.[15] However, the test for CEA is only effective in 4% and 25% of Stage I and II cancers, respectively, which is problematic for a cancer diagnostic because it is during these early stages when the disease is most effectively treated.[22]

The development and use of boronic acid functionalized synthetic lectins (SLs) for saccharide detection and cancer diagnosis is a rapidly growing field.[23–36] Boronic acids are incorporated into the SLs to enhance glycan binding *via* their ability to form covalent yet reversible bonds to the 1,2- and 1,3-diols present on many saccharides. These small molecule SLs generally show enhanced stability compared to antibodies and natural lectins, and it has been shown that incorporation of synthetic lectins into an array format allowed for the recognition and discrimination between simple monosaccharides and oligosaccharides in neutral aqueous media as well as real-world beverage samples, *i.e.* sweet tea with added Splenda.[37] Further advances using cross-reactive nanoparticle-conjugated polymer based arrays have shown utility in differentiating normal, cancerous and metastatic cell types.[38]

We previously described the design, synthesis and utility of boronic acid functionalized peptide-based SLs in binding to glycoproteins[36] and highlighted efforts in library design optimization and peptide sequencing.[35] SLs, that were both cross-reactive and up to 5-fold selective for a particular glycoprotein, were identified.

Herein, we report the identification and characterization of three additional SLs that bind to proof-of-concept glycoproteins with up to 50-fold selectivity, even in complex matrices (*i.e.*, human serum). Additionally, a four-component SL array was used to detect and differentiate five structurally similar cancer

associated glycans (Fig. 1), as well as one 'healthy' and six cancer cell lines with high classification accuracy. By combining selective and cross-reactive SLs within the array, the selectivity of an individual SL need not be high as each sensor need only be incrementally different to create an array that maximizes variation in the array response to different analytes.[39,40] Further analyses using directed partitioning, based on similarities in metastatic potential, was used to enhance the classification accuracy. Our results demonstrate the utility of using SL arrays for the diagnosis of cancer. Furthermore, since the analyte for which each SL was selected is not found on any of the cancerassociated cells studied, our array displays inherent adaptability.[39,40] That is to say that this relatively small array was able to "learn" and accurately classify never before seen analytes.[39,40]

Results and discussion

Employing the same approach used to identify SL1 and SL2,[35,36] SL3, SL4 and SL5 (Fig. 1B) were identified by screening our bead-based fixed position library with fluorescein isothiocyanate (FITC)-tagged versions of ovalbumin (OVA) and porcine stomach mucin (PSM). These SLs were subsequently re-synthesized and their selectivity and cross-reactivity evaluated using OVA, PSM, BSM (bovine submaxillary mucin) and BSA (bovine serum albumin). OVA, PSM and BSM are all glycoproteins, and it is noteworthy that the two mucins contain the same type of glycans but to differing extents and displayed in different environments. BSA, which is not glycosylated, was used as a control for non-specific protein binding.

SL selectivity studies

To control for differences in the extent of labeling or glycosylation, the fluorescence intensity of a similarly sized set of the SL library was used as a reference. The fluorescence intensity of the library was subtracted from the fluorescence intensity of the resynthesized SL incubated with the same FITC-tagged glycoprotein (Fig. S1, ESI†), providing a change in fluorescence intensity upon binding. A percent change in binding was obtained by dividing this difference by the fluorescence intensity
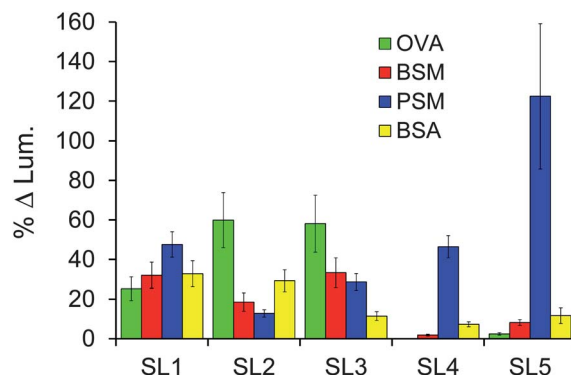

Fig. 2 Percent change in luminosity of each identified SL towards four different analytes (analyte identification indicated in the legends above). Error bars represent the standard error of the percent change relative to the control as this propagated uncertainty is based on the variance between replicate measurements for the sample and control reference.

of the library (Fig. 2). To compare the ability of each SL to differentially bind to glycoproteins, a selectivity factor was obtained by dividing the percent increase for each analyte by the percent increase of the weakest binder for that SL (Table 1). The library was chosen as the reference because it provides a control containing all of the potential cross-reactive elements that could interfere with our assessment of binding selectivity. Outliers from the control were removed using the studentized t-test at the second quartile to give an accurate average for standardization purposes.

The data for SL1 and SL2 have been previously described[35] and are included in Fig. 2 and Table 1 for comparison. Here we see that SL1 is completely cross-reactive, binding with no more than 2-fold selectivity for any one analyte. In contrast, SL2 shows modest selectivity for binding OVA. The 3- and nearly 5-fold selectivity SL2 shows over BSM and PSM, respectively, demonstrated the ability of this approach to distinguish between similar analytes. However the 2-fold selectivity of SL2 for OVA over BSA suggests high non-specific, background binding for this SL, thereby decreasing its potential utility in a diagnostic array.

The newly reported SL3 was selected from screening the library against OVA, and showed only 2-fold selectivity towards OVA over BSM and PSM, while exhibiting relatively low background binding, as indicated by the 5-fold selectivity over BSA. SL4 and SL5 were identified from screening the library for PSM binders. Although SL4 displays an impressive 25-fold selectivity for PSM over BSM, it exhibits only ~6-fold selectivity for PSM over BSA. Thus, while exhibiting some degree of selectivity and showing a particular preference for binding certain analytes (i.e., PSM vs. BSM), this SL can also be considered cross-reactive with respect to PSM vs. BSA. As such, this SL is an ideal candidate for inclusion in a sensor array because it possesses differential analyte binding. Note that SL4 shows virtually no affinity for OVA and as such the percent change in luminosity relative to the library control is very small (0.15%). Thus, for the discussion of selectivity, presented in Table 1, BSM was used as the weakest binder because it was not reasonable to use OVA and divide by such a small number (e.g. PSM selectivity vs. OVA is 250).

Similar to SL4, SL5 displayed exquisite selectivity, exhibiting 50-fold selectivity for PSM over OVA and ~15-fold selectivity over BSM. The excellent selectivity of SL4 and SL5 for PSM over

BSM (~25- and ~15-fold selectivity, respectively) is particularly impressive because these two glycoproteins possess identical types of glycans, though to a different extent and differentially displayed.[41–43] These results suggest that these SLs not only bind to the saccharide, but also the protein. Nevertheless, it is important to recognize that we have previously shown that glycans are significant for the SL–glycoprotein interaction.[36]

The robustness of the SL-glycoprotein interaction was assessed using SL2 and SL5 with differing percentages of human serum (0, 25, 50 and 95%) in screening buffer. Both SLs retained excellent selectivity for the respective glycoproteins in all concentrations of serum (Fig. S2, ESI†). Control experiments confirmed that no serum components caused any changes in the assay response (Fig. S3, ESI†). To examine the contribution of valency, dissociation constants (K_d) were determined for both the bead-based polyvalent SL5 and a monovalent SL5. The dynamic nature of the beads[44] (i.e., being a gel resin) allows for multiple interactions between bead-based SLs and the many glycans expressed on PSM. Therefore, incubating polyvalent, bead-based SL5 with varying concentrations of fluorescently labeled PSM (having a polyvalent display of glycans) yielded a K_d of 2.5 ± 0.29 μM (Fig. S4, ESI†).[45] A fluorescence polarization (FP) assay was used to measure the affinity of the fluorescently-labeled, monovalent SL5 (FITC-SL5) for PSM.[46] However, saturation of the FP signal was not observed because of limited glycoprotein solubility (Fig. S5, ESI†), thus K_d values could not be determined. Nevertheless, the observed response validated the assay and suggested that the K_d for the monovalent SL5-PSM interaction is significantly higher than 10 μM, the highest concentration tested. These results indicate that the polyvalent nature of the beads is critical for high affinity binding and suggest that multiple SLs on a single bead interact with each glycoprotein.

Glycan competition studies

Glycan competition assays were used to identify the glycan structure(s) that were responsible for SL2-OVA and SL5-PSM binding. For these studies, SL2 was selected over SL3 because of the higher selectivity shown for OVA over BSM and PSM, while SL5 was chosen over SL4 because of the larger signal intensity response. In this study, varying concentrations of different monosaccharides were independently incubated with equal portions of resin-bound SLs and a constant concentration of the FITC-glycoprotein (0.1 mg mL⁻¹) that the SL preferentially binds. The glycans used in the study of SL2 were those found on OVA, namely galactose, mannose and N-acetylglucosamine (GlcNAc).[36,47] For SL5, galactose, GlcNac, sialic acid, fucose and N-acetylgalactosamine (GalNAc),[36,48] which are all found on PSM, were used. Fructose was used to probe non-specific saccharide binding between the SLs and glycoproteins because it is one of the strongest known 1 : 1 boronic acid binders.[49,50] It was expected that effective competition between a monosaccharide and a FITC-glycoprotein, for binding to the resin-bound SL, would result in a decrease in luminosity. Such a decrease in the binding signal would suggest that a particular monosaccharide was important for glycoprotein binding to the SL. Note that the response values in Fig. 3 have been mathematically defined such that increasing bar height corresponds

Table 1 Selectivity factors for each SL screened against four different glycoproteins[a]

	OVA	BSM	PSM	BSA
SL1	1.0	1.3	1.9	1.3
SL2	4.7	1.4	1.0	2.3
SL3	5.1	2.9	2.5	1.0
SL4	0.1[b]	1.0	24.8	3.9
SL5	1.0	3.4	49.9	4.8

[a] The fold selectivity of an SL for one glycoprotein over another can be obtained by dividing their respective selectivity factors. SL1 and SL2 data from Bicker et al.[35] [b] The fold selectivity for SL4 was determined using BSM as the reference. OVA was not used as the reference because the %Δ luminosity was practically zero and dividing by such a small number resulted in fold selectivities that were quite meaningless.
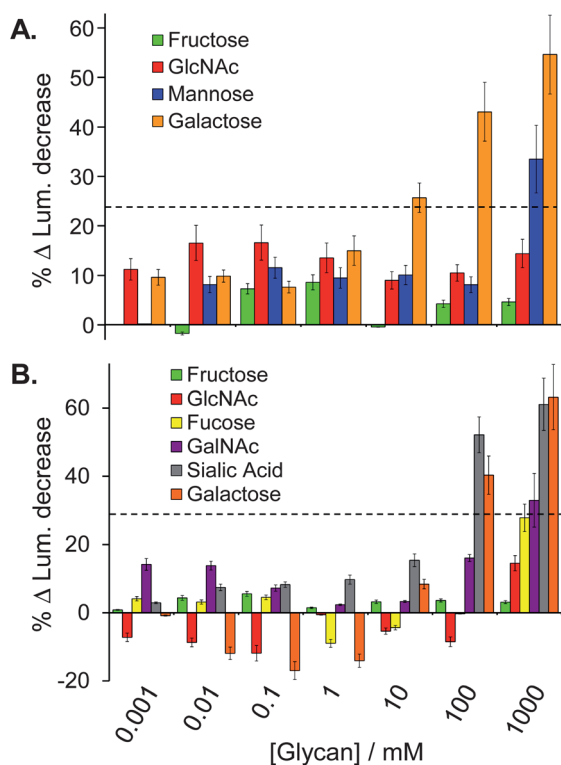
Fig. 3 Percent change in luminosity for the glycan competition studies used to explore the SL2-OVA (A) and SL5-PSM (B) binding interactions (analyte identification indicated in the legends above). Error bars represent the standard error of the percent change relative to the control as this propagated uncertainty is based on the variance between replicate measurements for the sample and control reference. The dashed lines in each panel indicate a competition threshold, based on three standard deviations above the noise. Signal response above this threshold indicates significant competition.

with more effective competition (intensity = (initial − final)/initial) to more clearly show the competition trends.

It is noteworthy that effective competition was only observed at high concentrations of the monovalent saccharides being studied. This result is likely due to the fact that these monosaccharide guests poorly compete with the multivalent display of saccharides found on the glycoproteins for binding to the multivalent display of SLs on the bead, as multivalent interactions are nearly always stronger than the sum of the monovalent interactions.[51] Also note that reducing glycosides and non-reducing monosaccharides (as found on the glycoproteins) were both used for these competition experiments, and that both classes of compounds showed similar trends in the data. The results from the competition studies with the reducing sugars are shown in Fig. 3 and the non-reducing sugar competition study data are summarized in the supporting information (Fig. S6, ESI†). Given that reducing monosaccharides can isomerize to the furanose form to provide a diol that more effectively binds to boronic acids in a 1 : 1 manner,[52–56] these monosaccharides provide a more stringent test of ligand binding than the non-reducing saccharides because they provide a "dual-competition" pathway. Namely *via* 1 : 1 furanose–boronic acid binding as well as the proposed pyranose–SL binding predicted for the

saccharides found on the glycoproteins. Note that significant competition was defined as being three standard deviations above the noise (indicated by the dashed lines in Fig. 3). For this analysis the standard error for 1000 mM galactose was used because it displays the largest variance, thus for SL2 and SL5, the 'cut-off' percent change in luminosity was 23% and 29%, respectively.

For SL2, no appreciable decrease in luminosity was observed with *N*-acetylglucosamine (GlcNAc) even at concentrations as high as 1 M (Fig. 3A, red bars) indicating that *N*-acetylglucosamine does not interact with SL2, and thereby suggesting that this glycan is not critical for binding SL2 to OVA. In contrast, a significant decrease in luminosity was observed with both 1 M mannose and with as little as 10 mM galactose (Fig. 3A, blue and orange bars, respectively). These data indicate that SL2 is likely binding primarily with galactose, and to a lesser extent with mannose, both found on OVA. Competitive binding with non-reducing saccharides also showed significant competition with mannose (see ESI†). These results are particularly impressive because they suggest that SL2 interacts with both terminal (galactose) and core (mannose) glycan structures.[47] Given that galactose is typically considered to be a weak boronic acid binder for simple 1 : 1 binding, the observed competition suggests that the binding site in this system is organized in a manner suitable for binding this sugar.[31]

Particularly small changes in luminosity corresponding to the addition of GlcNAc or fucose to SL5 (Fig. 3B, red and yellow bars, respectively) suggest that these glycans were not crucial for SL5 binding to PSM. Conversely, GalNAc competed for binding at high concentrations (Fig. 3B, purple bars), while both sialic acid and galactose displayed significant competition with PSM for binding to SL5 at concentrations above 100 mM (Fig. 3B, gray and orange bars, respectively), suggesting that SL5 is likely interacting with these terminal glycans. The data for the non-reducing sugars also demonstrates that sialic acid and GalNAc compete for binding to SL5.

The fructose competition studies are particularly impressive because neither SL2 nor SL5 showed any significant competition with up to 1 M saccharide, *i.e.*, less than 10% observed decrease in the glycoprotein binding signal (Fig. 3, green bars). Since fructose is one of the strongest known 1 : 1 binders for boronic acids, the lack of competition with fructose provides further evidence that the SL–glycoprotein interactions are likely multivalent.

Discrimination of glycans

As an initial test of our approach towards binding biologically relevant targets, we used an array of SL1, SL3, SL4 and SL5 to distinguish between five structurally similar cancer associated glycans (TF antigen, Le[a], Le[x], sLe[a] and sLe[x]; Fig. 1A). These glycans were chosen because they represent some of the more common saccharide motifs overexpressed by cancerous cells as well as being composed of many of the same monosaccharides that were used in the above competitive binding assay with our SLs. SL2 was not included in the array to eliminate redundancy based on response similarities with SL3 and because of the high background binding to BSA as compared with SL3. It is worth noting that while SL1 has higher background binding to BSA

than SL3; it was still included in the array due to its broad yet differential, cross-reactive response to all glycoproteins assessed.

After screening each SL against a solution containing biotinylated glycan and fluorescently labeled streptavidin, luminosity values, from fluorescence microscope images, were analyzed (4 SLs by 5 glycans by 15 replicates). To account for differences in bead size and loading levels, luminosities were normalized against the highest luminosity within a given SL type (in this study the greatest degree of variability stems from bead-to-bead variations). The unique pattern generated for each different glycan based on the response of the four different SLs is shown in Fig. 4A. Note that the response for each glycan produces patterns that do not differ greatly between analytes, nevertheless the response is reproducible and the resulting patterns are unique and distinguishable within the limits of the associated error.

Though these patterns are similar they are nonetheless unique, and therefore statistical analyses were used to identify the most significant features necessary for classification of the analytes. Specifically, linear discriminant analysis (LDA) was used.[57] This analysis minimized variation within each glycan type while maximizing the differences between different glycans by creating linear combinations of each response pattern and transforming them into canonical discriminants. For this analysis,

Fig. 4 Differentiation of five glycans using a SL array. (A) Fingerprint pattern of the average normalized luminosity intensities from SL1, SL3, SL4 and SL5 responding to five different glycans (TF, Le[a], Le[x], sLe[a] and sLe[x]). (B) The two-dimensional LDA score plot derived from the patterns shown in (A) for 15 replicates. Ellipses indicate 95% confidence level, analyte identification indicated in the legends above.

Discriminant 1 and Discriminant 2 contain 83.3% and 14.8% of the between group variation, respectively (Fig. 4B).[58] Therefore, each point in the plot contains information for an explicit measurement from the four different SLs responding to a specific glycan. Note that the different glycans are clustered into five groups with an average standard deviation of ∼6%. Furthermore, the Wilks' lambda value for this analysis is 0.009 with a p-tail value of <0.000001, indicating that there is a statistically significant difference in the population means from this analysis at the 95% level of confidence.

While there is some overlap of the ellipses drawn in Fig. 4B, it is important to recognize that this plot only shows two dimensions out of the four dimensional data used for this analysis (displaying the data in three dimensions (four is not possible) does not visually enhance the ability of the plot to show discrimination).

Leave-one-out cross-validation was next used to assess the ability of the SL array to classify unknowns as the appropriate glycan.[58] This procedure sequentially removes one sample point at a time and uses the remaining points as a new training set to create a model analogous to that shown in Fig. 4B. The classification accuracy was determined by whether or not the "left-out" data point was assigned to the correct glycan grouping. Using this method each analyte response can be used as an unknown and the classification accuracy determined for the entire data set. Based on this analysis, the SL array correctly classified 71 of the 75 measured samples (94.7% classification accuracy, with a chance accuracy of only 20%). Significantly, the Lewis antigens and their sialylated forms (Le[a]/Le[x] and sLe[a]/sLe[x]) were efficiently discriminated while only differing by the addition of a terminal sialic acid moiety. Additionally, this SL-array impressively distinguished between Le[a] and Le[x], as well as between sLe[a] and sLe[x], glycans where the only structural difference is the regiochemistry of the linkage to the core GlcNAc moiety (Fig. 1A). Of the four misclassified glycans (Table 2), Le[a] was twice identified as sLe[a], sLe[a] was once classified as Le[a], and Le[x] was once recognized as sLe[a].

To further evaluate the validity of our SL array for discriminating between these five structurally similar glycans, and to circumnavigate the disadvantages associated with leave-one-out cross-validation (also referred to as delete-one jackknife) the more statistically robust "boot-strapping" approach was used.[59]
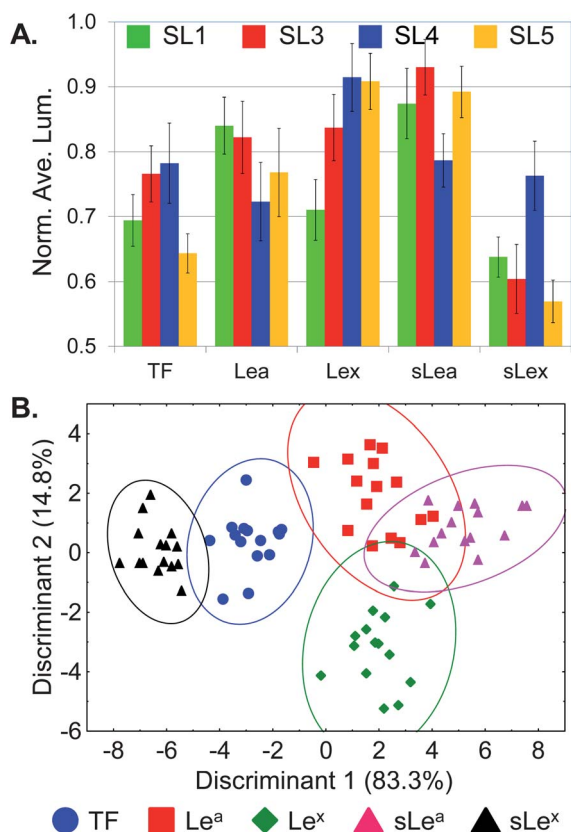
Table 2 Percent classification accuracies of glycans using an SL array as determined by different cross-validation techniques

	Jackknife	Boot-strap[a]	Training/test set[b]
Le[a]	86.6	85.8	88.2
Le[x]	93.3	95.3	96.0
TF	100	96.2	93.8
sLe[a]	93.3	93.6	94.4
sLe[x]	100	99.0	99.0
Total	94.6	94.2	93.9

[a] Average values were calculated from 50 replicate analyses of independently randomized samples with $N = 75$. [b] Average values were calculated from 25 replicate analyses of independently randomized samples at approximately 50% exclusion (randomized test samples accounted for, on average, 37 samples (49.5%), ranging from 26–43 samples).

In the approach, multiple data sets (typically 20–10 000) are generated by randomly selecting points from the original data set. During this sampling, the probability that a data point will appear 'n' times is close to a Poisson distribution with mean unity.

The Mersenne–Twister random number generator[60] was used for random selection of data points in Systat and data sets were created with 75 elements, the same number as the original data set. Fifty (50) separate and unique data sets were generated using this approach and were then evaluated for classification accuracy. Overall, this analysis yielded a $94.2 \pm 2.0\%$ classification accuracy for the array identifying these five glycans. This is consistent with the leave-one-out accuracy of 94.6%. Significantly, individual glycans were accurately classified from 86–99% (Table 2). As with the leave-one-out analysis, the three greatest misclassifications were due to Le^a being misclassified as sLe^a (9.3%), sLe^a being misclassified as Le^a (6.7%), and Le^x being misclassified as sLe^a (4.7%).

Still further stressing the limits of this array for differentiating glycans, we chose to randomly split our data in half. Using one half as a training set, to create a statistical model, and the other half as a test set to assess the ability of this model to accurately identify these "unknowns." Training and test sets were chosen at random from the Normal distribution.[61] To minimize systematic error, random set generation and subsequent analyses were carried out 25 times to create replicates. The data in Table 2 represents the averages obtained for these replicate runs. Consistent with the previously described analyses, the overall classification accuracy of this approach was $93.9\% \pm 2.8\%$. This is by far the most stringent method used to assay the validity of the models generated from our SL array and still exhibits exceptional classification accuracy. The consistency displayed across the three methods further testifies to the strength of the outlined SL array design for discriminating structurally similar cancer associated glycans.

As indicated above, it is possible that the SLs interact, not only with the glycan, but also with the protein portion of glycoproteins. In this analysis the protein component, FITC-streptavidin, is the same for each glycan being analyzed. As such, any observed difference in the response from the array must be attributed to the glycan constituent. Given the structural similarities between these glycans, it is remarkable that there were not more misclassifications. In total, these results validate our ability to differentiate structurally similar cancer associated glycans with high accuracy using a small, cross-reactive SL array.

Discrimination of cancer cell lines

To further probe the utility of this four-component SL-array, we targeted an important goal in cancer diagnostics: to distinguish between healthy, cancerous/non-metastatic and cancerous/metastatic cell types. Specifically, we used our SL-array to discriminate between seven different cell types including: three colorectal carcinoma non-metastatic cell lines (HCT116, CT-26, HT-29), three colorectal carcinoma metastatic cell lines (CT-26-F1, CT-26-FL3, LoVo), and one murine fibroblast cell type (NIH/3T3) to serve as a "healthy" control cell line. Note that CT-26-F1 and FL3 cell lines were derived from the parental CT-26 cell line by *in vivo* education selection through serial passage in Balb/c mice and represent a series of highly similar isogenic cell lines that only differ in their metastatic potential (CT-26 <10% metastatic, CT-26-F1 ~50% metastatic and CT-26-FL3 ~95% metastatic).

Unlike the identification of discrete, structurally similar glycans, we predicted that cell type discrimination would result from a general response to the distinctive membrane protein composition of each cell type, thus affording a unique cellular signature, as previously demonstrated by Bunz and Rotello.[38] For this study, cell membrane proteins and glycoproteins were isolated[62] and fluorescently labeled to detect binding to the SL-array. While we note that this labeling approach is less than ideal for the development of a diagnostic, it does suffice to demonstrate the utility of using an SL array towards discriminating between cell lines. To account for differences in the extent of fluorescent labeling and protein concentration between each cell extract, luminosities were normalized against the highest luminosity within a given cell type (in this study the greatest degree of variability stems from cell line-to-cell line variations).[63] Note that replicates obtained for the LoVo, HCT116, NIH/3T3 and HT-29 cells were derived from multiple sample preparations of cell cultures grown by different researchers over the course of several months.

Fig. 5A shows the two-dimensional projection of the LDA results (4 SLs by 7 cell lines by 40 replicates each for NIH/3T3, CT-26, HT-29, CT-26-F1 and CT-26-FL3; 60 replicates for LoVo; and 80 replicates for HCT116). It is important to note that if all of the variance is captured in one discriminant then the statistical analysis is not really necessary; however successive discriminants containing large portions of the variance supports the validity of and the need for the statistical analysis. In this analysis Discriminant 1 contains 54% and Discriminant 2 contains 31% of the total variance, while the remaining 15% is partitioned between Discriminants 3 (11%) and 4 (4%) (*i.e.*, this is four-dimensional data). This distribution of variance suggests that each of the SLs in the array is important for discriminating between cell lines.

Note that each of the same colored points cluster together indicating the ability of the statistical model to define similarity between replicates of a specific analyte. However, some of these different clusters are closely packed and some groups overlap suggesting that there are strong similarities between some of the analytes, as would be expected. Nevertheless, it important to recognize that the data is in fact four dimensional; therefore the overlap between groups shown in this two dimensional figure (Fig. 5A) is not necessarily indicative of poor classification.

To quantitatively evaluate the accuracy of this approach, leave-one-out cross-validation was used and demonstrated that this statistical model exhibited 92.1% accuracy, correctly identifying 313 out of 340 measured samples. Fig. 5B presents the LDA classification results matrix for the assay. The cross-diagonal of the matrix corresponds to the number of accurately identified samples (set in bold). Any numbers that fall off this diagonal represent the number of misclassifications for that cell type and correspond to the misclassified cell type identity. The column on the right of the matrix provides the classification accuracy for each cell type. While the overall classification accuracy for the array is 92.1%, the accuracy for each individual cell type varies between 81–100%.
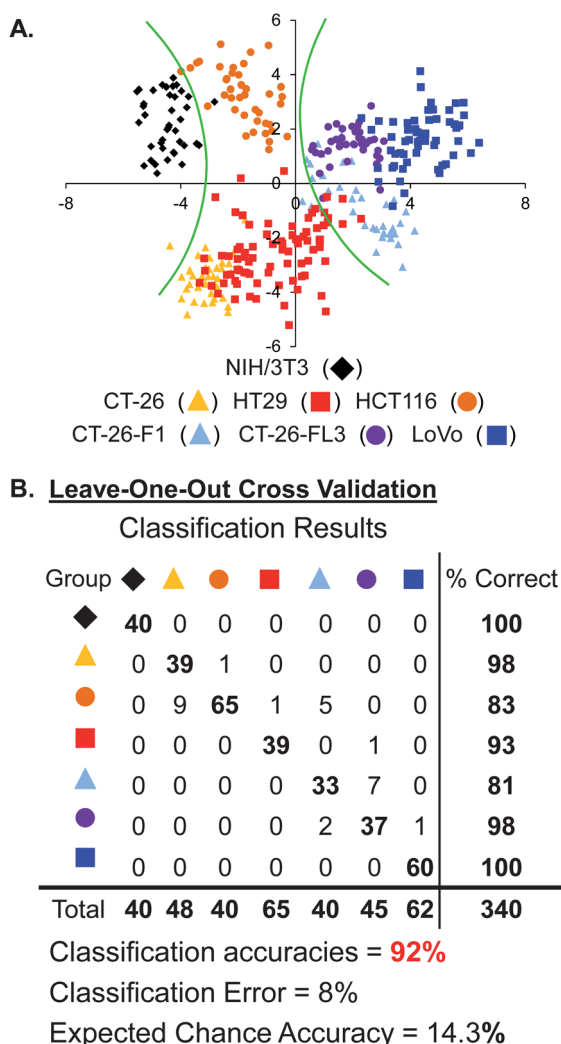
Fig. 5 (A.) The two-dimensional LDA score plot of the response of the SL array for discriminating seven cell types. Green curves indicate boundaries between healthy, cancerous/non-metastatic and cancerous/metastatic cell types. For clarity, the Discriminant 1 *vs.* Discriminant 2 data was rotated 20° about the *z*-axis (analyte identification indicated in the legends above). (B.) Leave-one-out cross validation classification matrix for the SL-array based assay.

Given the diversity of protein and glycan structures present on the cell membrane for each of these different cell types, it is difficult to speculate on the specific glycans that are recognized by the SLs and that contribute to the discrimination of these different cell lines. Still, there are clear trends in the statistical output that support the validity of this analysis. As one moves from left to right along the *x*-axis in Fig. 5A the metastatic potential of the cell lines increases. Specifically, the green curves in Fig. 5A provide boundaries between the "healthy" 3T3 cells (black) at the far left of this plot; the cancerous/non-metastatic cell lines (HCT116, CT-26 and HT-29 – orange, yellow, red, respectively) in the middle and the cancerous/metastatic cell lines (CT-26-F1, CT-26-FL3 and LoVo – light blue, purple, blue, respectively) to the right. This clustering of cell types with similar metastatic potential suggests that the basis upon which the first two discriminants are derived correlate highly with this attribute.

Additionally, the Wilks' lambda value for this analysis is 0.003 with a p-tail value of <0.000001, thus indicating that there is a statistical difference in the population means from this analysis at the 95% level of confidence. Further MANOVA treatment of the data provided a Wilks' lambda value of 0.004 with a p-value of <0.000001 and sequential univariate F-Tests for each variable provided p-values of <0.000001 for each.

To further validate this approach, boot-strapping and training/test set analyses (at a 50% exclusion split) were carried out. The results provided in Table 3 indicate that these more rigorous validation methods provide classification accuracies consistent with those obtained for the leave-one-out cross-validation, 92.1 ± 1.1% and 92.7 ± 1.8%, respectively. As seen for the glycan analysis above, cell-line misclassifications were consistent across all three validation methods. Furthermore, the misclassified cell-lines were not random but often had a structural basis behind the result. For example, in the boot-strap analysis, CT-26-F1 displayed the lowest classification accuracy at 80.5%; and all of the misclassifications were as CT-26-FL3, an isogenic, highly metastatic cell line. Similarly, from the training/test set analysis, CT-26-FL3 has one of the lower classification accuracies (87.4%); here all of the misclassifications in this analysis were attributed to CT-26-F1 (85%) and LoVo (15%). Recall that both CT-26-FL3 and LoVo are highly metastatic and that CT-26-FL3 is isogenic with CT-26-F1. Finally, while the classification error for HCT116 is relatively large across the validation methods (classification accuracies from 81.3–89.2%), the majority of misclassifications are CT-26 and HT-29 cells. Since all three cell lines are cancerous non-metastatic, these misclassification are not unexpected because classification accuracy, in this model, correlates with metastatic potential.

Directed partitioning for enhanced cancer cell discrimination

With the advancement of cross-reactive sensor arrays, numerous statistical and non-statistical approaches have become available to evaluate the array responses; however, many do not scale well with increasing numbers of analyte classes. For analysis of these multi-class systems, the most common statistical approaches rely on multivariant analysis, such as feature selection algorithms. Alternatively, the analysis can be reduced to a series of multiple

Table 3 Percent classification accuracies of cell lines using an SL array as determined by different cross-validation techniques

	Jackknife	Boot-strap[a]	Training/test set[b]
3T3/NIH	100	100	100
CT-26	97.5	97.0	96.7
CT-26-F1	82.5	80.5	82.3
CT-26-FL3	92.5	92.7	87.4
HCT116	81.3	83.6	89.2
HT-29	97.5	96.8	96.7
LoVo	100	99.9	100
Total	92.1	92.1	92.7

[a] Average values were calculated from 100 replicate analyses of independently randomized samples with $N = 340$. [b] Average values were calculated from 25 replicate analyses of independently randomized samples at approximately 50% exclusion (randomized test samples accounted for, on average, 173 samples (50.9%), ranging from 153–191 samples).

binary classification problems run in parallel, such as one-from-n (one-against-rest), pairwise (one-against-one) or hierarchical (decision trees) processes.

We have previously presented a hybrid approach, for the identification and discrimination of biogenic amines,[64] where the multi-class system is simplified in a manner analogous to the binary classification routines. However, this class reduction did not rely on statistical methods; instead, we used insight into the chemical nature of the analytes to group these compounds into structurally related categories.

In training the array using this directed partitioning technique, previous knowledge about the nature of the samples is required, for example whether the cell lines are cancerous or not. However, as described above, no specific information about the exact identity of the analytes is necessary, for example the glycan being bound. This method is in direct contradiction with traditional routines that rely solely on statistical models. The quality of the results from this approach is often enhanced because logical reasoning, based on the inherent nature of the samples, is involved as part of the partitioning. Once classified into groups, these subsets could be further categorized as the individual components using a hierarchical, group–ungroup, multi-layered analysis approach to achieve enhanced classification. Therefore, directed partitioning was used to reduce classification error and the data were grouped according to their metastatic potential, *i.e.* healthy, cancerous/non-metastatic and cancerous/metastatic.

When the analysis was performed using these new groups, classification accuracies, based on leave-one-out cross-validation, improved to 97.1%, correctly identifying 330 out of 340 samples (Fig. 6A). The classification accuracy is unchanged using the training/test set analysis at 50% exclusion (97.3 ± 1.5%). From a diagnostic perspective, this is perhaps the most important classification; to determine whether the cancer is present or not. Of the 10 misclassified samples, 8 were cancerous/non-

metastatic that were identified as cancerous/metastatic and the remaining 2 were cancerous/non-metastatic that were considered healthy, thus producing a 0.6% "false negative" rate. Additionally, note that the data for the 3T3 cells seems "bimodal," showing two distinct clusters within the category. This separation results from combining data acquired by different experimentalists from different culture broths. Most significantly, while this separation is noticeable, the overall clustering is still quite tight and the 3T3 classification is 100% in the leave-one-out analysis. Based on the training/test set analysis, the within group misclassification is 6.7%, resulting in an overall 0.8% "false-positive" rate. These results clearly support the validity of this approach to identify cancerous from noncancerous cell lines. Furthermore, the low false negative rate compares quite favorably with current diagnostic tests such as the CEA test, where the false negative rate is 16%.[22]

By successively ungrouping each subset, a multi-layered analysis could be carried out to identify the individual cell type. The two-dimensional projections of the four-dimensional LDA results for these subset categorizations are shown in Fig. 6B–C. In Fig. 6B cancerous/non-metastatic cell lines were accurately discriminated in 150 out of 160 samples or 94%; an improvement from 89% in the single-layer analysis. Specifically, HT-29 cells were classified with 100% accuracy; CT-26 cells achieved 98% classification accuracy and HCT116 were classified with 89% accuracy. For the 10 misclassified analytes, 9 of the HCT116 samples were identified as CT-26 while one CT-26 was classified as HCT116. Given that all three of these cell lines are cancerous non-metastatic, these misclassification are not extraordinary because classification accuracy, in this model, correlates with metastatic potential.

Similarly, the cancerous/metastatic cell lines were separated into the individual components with 92% classification accuracy (129 out of 140 samples, Fig. 6C). In this analysis, 91% of the misclassifications resulted from mis-assignments between CT-26-F1 and CT-26-FL3. It is important to recall that these are highly similar isogenic cell lines, derived from the parental CT-26 cell line, and differ only in their metastatic potential. The impressive 88% classification accuracy, between the highly metastatic cell lines CT-26-F1 and CT-26-FL3, as well as 92% classification accuracy between the parent CT-26, and metastatic CT-26-F1 and CT-26-FL3 cell lines further validates our approach while indicating that there are distinct glycosylation patterns associated with metastatic potential. These results highlight the adaptability of this array-based approach for classifying cell types based on complex mixtures rather than a specific analyte, thereby mimicking the mammalian senses of taste and smell.[39,40]

Conclusions

In summary, selective and cross-reactive SLs have been identified by screening a resin-based SL library binding to glycoproteins. Selectivities as high as ~50-fold, for one glycoprotein over another, have been observed. The selectivity of the SL-glycoprotein interactions are maintained in 95% human serum, demonstrating their robustness. Significantly, SLs were assembled into an array format to distinguish between five structurally similar cancer associated glycans with 94% accuracy. Additionally, the same array was used to discriminate seven cell types,
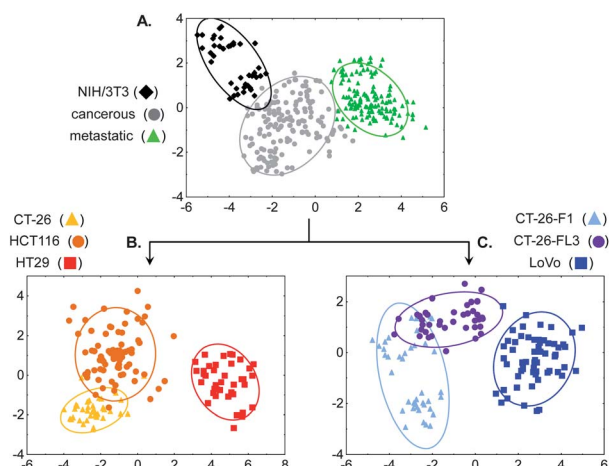

Fig. 6 (A) The 2-D LDA score plot of the response of the SL array for discriminating grouped healthy, grouped cancerous/non-metastatic and grouped cancerous/metastatic cell types. (B) 2-D LDA score plot of the array response to ungrouping the cancerous/non-metastatic cells: HCT116, CT-26 and HT-29. (C) 2D LDA score plot of the array response to ungrouping the cancerous/metastatic cells: CT-26-F1, CT-26-FL3 and LoVo. Ellipses indicate 95% confidence level, analyte identification indicated in the legends above.

including three colorectal carcinoma non-metastatic cell lines, three colorectal carcinoma metastatic cell lines, and one healthy control cell line with high accuracy. Two statistical methods were employed for this analysis. In a single layered approach, analysis of all seven analytes at once provided overall classification accuracy above 92%. Using directed partitioning afforded 97% accuracy for distinguishing between cancerous non-metastatic, cancerous metastatic and healthy cells. By sequentially ungrouping these subsets the overall accuracy of the analysis was improved compared with the single-layer analysis. Current work is focused on identifying SLs for specific cancer associated targets to enhance detection sensitivity and discrimination ability, as well as expanding the array to discriminate between other glycans and cell types. Finally, we note that SLs themselves may possess therapeutic utility as targeting agents and metastatic inhibitors, as has been shown with natural lectins.[65,66]

Notes and references

1 D. H. Dube and C. R. Bertozzi, *Nat. Rev. Drug Discovery*, 2005, **4**, 477–488.
2 V. Harmat and G. Naray-Szabo, *Croat. Chim. Acta*, 2009, **82**, 277–282.
3 J. J. Lavigne and E. V. Anslyn, *Angew. Chem., Int. Ed.*, 2001, **40**, 3118–3130.
4 F. P. Schmidtchen, *Chem. Soc. Rev.*, 2010, **39**, 3916–3935.
5 A. P. Umali and E. V. Anslyn, *Curr. Opin. Chem. Biol.*, 2010, **14**, 685–692.
6 J.-P. Behr, The Lock and Key Principle: The State of the Art 100 Years on, in *Perspect. Supramol. Chem.*, 1994; 1.
7 M. Brattoli, G. de Gennaro, V. de Pinto, A. D. Loiotile, S. Lovascio and M. Penza, *Sensors*, 2011, **11**, 5290–5322.
8 M. Cole, J. A. Covington and J. W. Gardner, *Sens. Actuators, B*, 2011, **156**, 832–839.
9 R. Paolesse, D. Monti, F. Dini and C. Di Natale, *Top. Curr. Chem.*, **300**, 139–174.
10 R. K. Ranjan and K. Prasad, *Anal. Chem–Indian J.*, 2008, **7**, 739–742.
11 F. Roeck, N. Barsan and U. Weimar, *Chem. Rev.*, 2008, **108**, 705–725.
12 A. D. Wilson and M. Baietto, *Sensors*, 2009, **9**, 5099–5148.
13 J. Yinon, *Anal. Chem.*, 2003, **75**, 98A–105A.
14 M. A. Hollingsworth and B. J. Swanson, *Nat. Rev. Cancer*, 2004, **4**, 45–60.
15 T. Nakagoe, T. Sawai, T. Tsuji, M. A. Jibiki, A. Nanashima, H. Yamaguchi, T. Yasutake, H. Ayabe and K. Arisawa, *Hepatogastroenterology*, 2003, **50**, 696–699.
16 W. S. Wang, J. K. Lin, T. C. Lin, T. J. Chiou, J. H. Liu, C. C. Yen, W. S. Chen, J. K. Jiang, S. H. Yang, H. S. Wang and P. M. Chen, *Hepatogastroenterology*, 2002, **49**, 388–392.
17 J. L. Magnani, *Arch. Biochem. Biophys.*, 2004, **426**, 122–131.
18 S. E. Baldus, T. K. Zirbes, S. P. Monig, S. Engel, E. Monaca, K. Rafiqpoor, F. G. Hanisch, C. Hanski, J. Thiele, H. Pichlmaier and H. P. Dienes, *Tumor Biol.*, 1998, **19**, 445–453.
19 M. M. Fuster, J. R. Brown, L. Wang and J. D. Esko, *Cancer Res.*, 2003, **63**, 2775–2781.
20 J.-i. Ogawa, A. Sano, S. Koide and A. Shohtsu, *J. Thorac. Cardiovasc. Surg.*, 1994, **108**, 329–336.
21 S. Nakamori, M. Kameyama, S. Imaoka, H. Furukawa, O. Ishikawa, Y. Sasaki, Y. Izumi and T. Irimura, *Dis. Colon Rectum*, 1997, **40**, 420–431.
22 M. G. Fakih and P. Aruna, *Oncology*, 2006, **20**, 579–587.
23 D. Walker, G. Joshi and A. Davis, *Cell. Mol. Life Sci.*, 2009, **66**, 3177–3191.
24 S. Jin, Y. Cheng, S. Reid, M. Li and B. Wang, *Med. Res. Rev.*, 2010, **30**, 171–257.
25 T. D. James, K. R. A. S. Samankumara and S. Shinkai, *Angew. Chem., Int. Ed.*, 1997, **35**, 1911–1922.
26 T. D. James and S. Shinkai, *Top. Curr. Chem.*, 2002, **218**, 159–200.
27 J. J. Lavigne and E. V. Anslyn, *Angew. Chem., Int. Ed.*, 1999, **38**, 3666–3669.
28 M. Li, N. Lin, Z. Huang, L. Du, C. Altier, H. Fang and B. Wang, *J. Am. Chem. Soc.*, 2008, **130**, 12636–12638.
29 Yamamoto, M. M. Takeuchi and S. Shinkai, *Tetrahedron*, 1998, **54**, 3125–3140.
30 W. Yang, H. Fan, X. Gao, S. Gao, V. V. R. Karnati, W. Ni, W. B. Hooks, J. Carson, B. Weston and B. Wang, *Chem. Biol.*, 2004, **11**, 439–448.
31 T. D. James, M. D. Phillips and S. Shinkai, *Boronic acids in saccharide recognition*, Royal Society of Chemistry, Cambridge, UK, 2006.
32 P. J. Duggan and D. A. Offermann, *Tetrahedron*, 2009, **65**, 109–114.
33 A. Pal, M. Bérubé and D. G. Hall, *Angew. Chem., Int. Ed.*, 2010, **49**, 1492–1495.
34 T. D. James, H. Shinmori and S. Shinkai, *Chem. Commun.*, 1997, 71–72.
35 K. L. Bicker, J. Sun, J. J. Lavigne and P. R. Thompson, *ACS Comb. Sci.*, 2011, **13**, 232–243.
36 Y. Zou, D. L. Broughton, K. L. Bicker, P. R. Thompson and J. J. Lavigne, *ChemBioChem*, 2007, **8**, 2048–2051.
37 N. Y. Edwards, T. W. Sager, J. T. McDevitt and E. Anslyn, *J. Am. Chem. Soc.*, 2007, **129**, 13575–13583.
38 A. Bajaj, O. R. Miranda, I.-B. Kim, R. L. Phillips, D. J. Jerry, U. H. F. Bunz and V. M. Rotello, *Proc. Natl. Acad. Sci. U. S. A.*, 2009, **106**, 10912–10916, S10912/10911–S10912/10910.
39 J. J. Lavigne and E. V. Anslyn, *Angew. Chem., Int. Ed.*, 2001, **40**, 3118–3130.
40 A. T. Wright and E. V. Anslyn, *Chem. Soc. Rev.*, 2006, **35**, 14–28.
41 N. G. Karlsson, H. Nordman, H. Karlsson, I. Calstedt and G. C. Hansson, *Biochem. J.*, 1997, **326**, 911–917.
42 S. M. D'Arcy, C. M. Donoghue, C. A. Koeleman, D. H. V. d. Eijnden and A. V. Savage, *Biochem. J.*, 1989, **260**, 389–393.
43 S. Martensson, S. B. Levery, T. T. Fang and B. Bendiak, *Eur. J. Biochem.*, 1998, **258**, 603–622.
44 *Combinatorial Chemistry Catalog and Solid Phase Organic Chemistry (SPOC) Handbook*, Novabiochem, Laufelfingen, 1996.
45 *GraFit*, Erithacus Software Limited, Version 5.0.11 edn, 2004. Note that when the data were fit to a two-site binding model no significant differences in the calculated K_d values were apparent, $K_{d}1 = 0.47 \pm 40.51$ μM and $K_{d}2 = 43.47 \pm 41.40$ μM. However, the errors are quite large for this later analysis while the single site model afforded a significantly better fit to the data.
46 N. J. Moerke, *Curr. Protoc. Chem. Biol.*, 2009, **1**, 1–15.
47 D. J. Harvey, D. R. Wing, B. Kuster and I. B. Wilson, *J. Am. Soc. Mass Spectrom.*, 2000, **11**, 564–571.
48 K. T. Pilobello, L. Krishnamoorthy, D. Slawek and L. K. Mahal, *ChemBioChem*, 2005, **6**, 985–989.
49 G. Springsteen and B. Wang, *Tetrahedron*, 2002, **58**, 5291–5300.
50 S. Jin, C. Zhu, Y. Cheng, M. Li and B. Wang, *Bioorg. Med. Chem.*, 2010, **18**, 1449–1455.
51 M. Mammen, S.-K. Choi and G. M. Whitesides, *Angew. Chem., Int. Ed.*, 1998, **37**, 2754–2794.
52 M. Bielecki, H. Eggert and J. C. Norrild, *J. Chem. Soc., Perkin Trans. 2*, 1999, 449–456.
53 S. P. Draffin, P. J. Duggan, S. A. M. Duggan and J. C. Norrild, *Tetrahedron*, 2003, **59**, 9075–9082.
54 H. Eggert, J. Frederiksen, C. Morin and J. C. Norrild, *J. Org. Chem.*, 1999, **64**, 3846–3852.
55 J. C. Norrild and H. Eggert, *J. Am. Chem. Soc.*, 1995, **117**, 1479–1484.
56 J. C. Norrild and H. Eggert, *J. Chem. Soc., Perkin Trans. 2*, 1996, 2583–2588.
57 *Systat*, Version 11.00.01, Systat Software, Inc., 2004.
58 K. R. Beebe, R. J. Pell and M. B. Seasholtz, *Chemometrics. A Practical Guide.*, John Wiley & Sons, Inc., New York, 1998.

59 C. F. J. Wu, *Ann. Stat.*, 1986, **14**, 1261–1295.
60 M. Matsumoto and T. Nishimura, *ACM Transactions on Modeling and Computer Simulation*, 1998, **8**, 3–30.
61 G. Casella and R. L. Berger, *Statistical Inference*, Thomas Learning, Pacific Grove, CA, 2002.
62 T. Nakamura, T. Hayashi, Y. Nishimura-Nasu, F. Sakaue, Y. Morishita, T. Okabe, S. Ohwada, K. Matsuura and T. Akiyama, *Genes Dev.*, 2008, **22**, 1244–1256.
63 Control studies were carried out to assure that the array response was independent of concentration or extent of glycoprotein labeling with the fluorophore.
64 T. L. Nelson, I. Tran, T. G. Ingaliinera, M. S. Maynor and J. J. Lavigne, *Analyst*, 2007, **132**, 1024–1030.
65 G. Mannori, D. Santoro, L. Carter, C. Corless, R. M. Nelson and M. P. Bevilacqua, *Am. J. Pathol.*, 1997, **151**, 233–242.
66 T. Minko, *Adv. Drug Delivery Rev.*, 2004, **56**, 491–509.